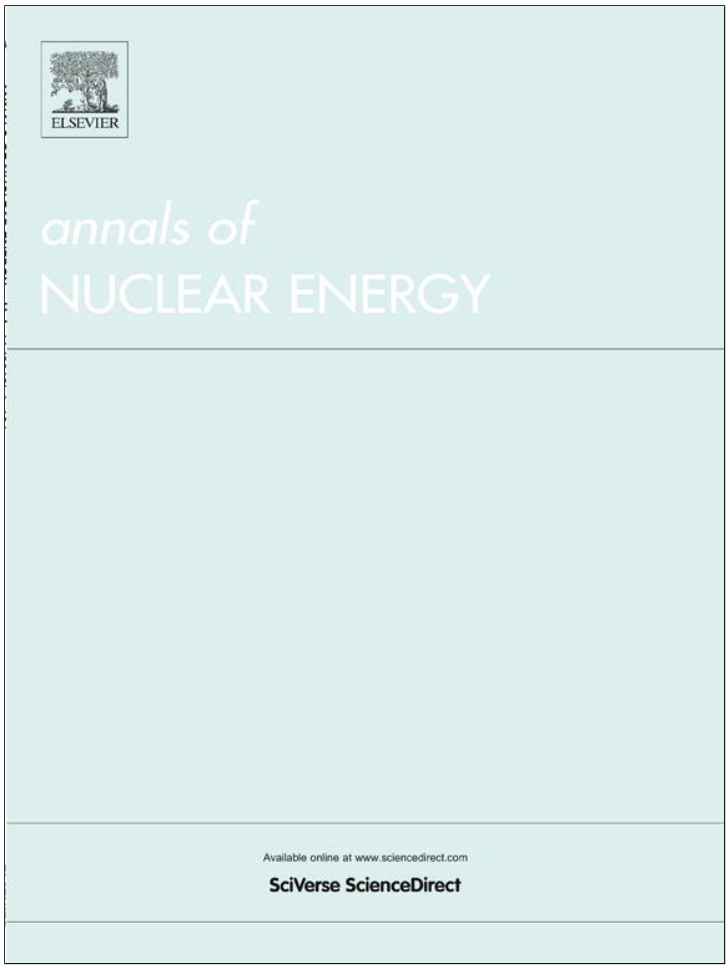

(This is a sample cover image for this issue. The actual cover is not yet available at this time.)

Annals of Nuclear Energy 50 (2012) 18–32

Contents lists available at SciVerse ScienceDirect

Annals of Nuclear Energy

journal homepage: www.elsevier.com/locate/anucene

Verification of analytic energy moments for the one-dimensional energy dependent neutron diffusion equation with MCNP5 and Attila-7.1.0

Douglas S. Crawford [a,*], Terry A. Ring [b]

[a] Center for Space Nuclear Research/Idaho National Lab, 995 University Blvd, Idaho Falls, ID 83402, USA
[b] University of Utah, Chemical Engineering Department, 50 S. Central Campus Dr., Rm 3290, Salt Lake City, UT 84112, USA

ARTICLE INFO

Article history:
Received 21 January 2012
Received in revised form 26 June 2012
Accepted 27 June 2012

Keywords:
Energy moments
Statistics moments
Neutron diffusion
MCNP5
Attila

ABSTRACT

The energy dependent neutron diffusion equation (EDNDE) is converted into a moment equation which is solved analytically for the 1-D problem of a bare sphere of pure ^{235}U. The normalized moments 0–5 generated analytically are compared to normalized energy moments, from Monte Carlo N Particle 5 version 1.40 (MCNP5) and Attila-7.1.0-beta version (Attila). The analytic normalized neutron energy moments, fall between the results from MCNP5 (lower bound) and Attila (upper bound) and are accurate compared to MCNP5 neutron energy moments when error in this Monte Carlo simulation are considered. The error range is from 0% to 14%. The Attila moments are less accurate when compared to MCNP5 than the analytical moments derived in this work. The method of moments is shown to be a fast reliable method, compared to either Monte Carlo methods (MCNP5) or 30 multi-energy group methods (Attila).

Introduction

Solving for neutron energy distributions in nuclear reactors is complex and has been studied with various methods, mostly numerical in nature (Cho, 2008). The main difficulty in solving for neutron distributions lies in solving the neutron transport equation, (Duderstadt and Hamilton, 1976, p. 114). The complexities and difficulties in trying to solve the transport equation arise because it depends on seven variables: energy of the neutrons (E), angle of neutron travel (θ and ϕ), space (x, y and z) and time (t). Simplifications are made to create a more easily solvable equation, but numerical methods are still necessary to solve for neutron fluxes and populations (Lewis and Miller, 1993).

The success of quadrature method of moments (QMOM) for particles is encouraging and has motivated the work presented here. QMOM has been shown to be an excellent method to solve partial integro-differential equations for particle population balances (Marchisio et al., 2003), aerosols (McGraw, 1997), and suspended particles in a fluid within computational fluid dynamics codes (Bin-Wan and Ring, 2006), (Marchision et al., 2003). The particle equations in question are similar mathematically to the EDNDE. The EDNDE is shown in Eq. (1). This is the first attempt to verify the method of moments as an accurate solution to EDNDE. Once the method of moments is proven successful, QMOM may be used to drastically reduce the computational burden in multi-physics problems that include neutron transport.

$$\frac{1}{v}\frac{\partial\phi(\vec{r},E,t)}{\partial t} - \nabla D(\vec{r},E)\nabla\phi(\vec{r},E,t) + \Sigma_t(\vec{r},E)\phi(\vec{r},E,t) = \int_0^\infty \Sigma_s(\vec{r},E\to\acute{E})\phi(\vec{r},\acute{E},t)d\acute{E} + \chi(E)\int_0^\infty \nu(\acute{E})\Sigma_f(\vec{r},\acute{E})\phi(\vec{r},\acute{E},t)d\acute{E} \quad (1)$$

The method of moments (MOM) approach solves for the moments of a distribution instead of the distribution itself. MOM can be considered to be a deterministic method to find stochastic parameters. The neutron flux can be treated as a probability density function (PDF), where the normalized moments provide the mean, variance, skewness and kurtosis (Kenny, 1947) of the flux so once the moments are solved for they can be put into the correct PDF to reproduce the flux. Mathematically the mean, variance, skewness and kurtosis (Casella and Berger, 2002) for the energy variable of the neutron flux are represented here where ϕ in Eqs. (2)–(5) represent the energy dependent neutron flux $\phi(\vec{r},E,t)$:

$$mean = \frac{\int_0^\infty E*\phi dE}{\int_0^\infty \phi dE}, \quad (2)$$

$$variance = \frac{\int_0^\infty E^2*\phi dE}{\int_0^\infty \phi dE}, \quad (3)$$

$$skewness = \frac{\int_0^\infty E^3*\phi dE}{\int_0^\infty \phi dE} \quad (4)$$

$$kurtosis = \frac{\int_0^\infty E^4*\phi dE}{\int_0^\infty \phi dE} \quad (5)$$

* Corresponding author. Tel.: +1 8015051409.
E-mail address: douglas.crawford@inl.gov (D.S. Crawford).

0306-4549/$ - see front matter © 2012 Elsevier Ltd. All rights reserved.
http://dx.doi.org/10.1016/j.anucene.2012.06.022

Table 1
Energy group structure for Attila-7.1.0-beta.

Group, #	Energy range, MeV		Group, #	Energy range, MeV		Group, #	Energy range, MeV	
1	2.00E+01	1.70E+01	11	7.79E+00	6.87E+00	21	8.21E−01	2.35E−01
2	1.70E+01	1.60E+01	12	6.87E+00	6.07E+00	22	2.35E−01	6.74E−02
3	1.60E+01	1.50E+01	13	6.07E+00	5.35E+00	23	6.74E−02	1.93E−02
4	1.50E+01	1.39E+01	14	5.35E+00	4.72E+00	24	1.93E−02	5.53E−03
5	1.39E+01	1.30E+01	15	4.72E+00	3.68E+00	25	5.53E−03	3.54E−04
6	1.30E+01	1.20E+01	16	3.68E+00	2.87E+00	26	3.54E−04	2.26E−05
7	1.20E+01	1.10E+01	17	2.87E+00	2.23E+00	27	2.26E−05	3.47E−06
8	1.10E+01	1.00E+01	18	2.23E+00	1.74E+00	28	3.47E−06	6.25E−07
9	1.00E+01	8.82E+00	19	1.74E+00	1.19E+00	29	6.25E−07	1.24E−08
10	8.82E+00	7.79E+00	20	1.19E+00	8.21E−01	30	1.24E−08	1.00E−11

The starting point for the analysis is the EDNDE, we have assumed diffusion theory is applicable and consider only the 1-D analytic case, a bare sphere. The same analysis can be applied to an infinite slab as well with similar results. Neutron diffusion theory is well documented in literature; (Duderstadt, 1976, Foster, 1977, Lamarsh, 2001, Lewis, 1993, Weinberg, 1958, etc.) and is not discussed in detail here. An average angle of scatter for the neutrons (μ) is also assumed. This method does not assume any distribution to develop the cross-sections or a specific spectrum for fission as a weighting value per energy group, which makes this method very unique, the analysis does cut off at 10 MeV since this value captures 100% of the fission spectrum and the neutron flux above that energy is very small and assumed to be negligible.

This paper is focused on deriving and comparing analytic moments from the energy dependent neutron diffusion equation (EDNDE) Eq. (1), with energy moments generated from MCNP5 (MCNP) and Attila 7.1.0-beta (Attila), which both are full neutron transport codes. This seems like an apples and oranges comparison, since this is a comparison between transport and analytic EDNDE moments, but it is necessary because the Monte Carlo method used in Los Alamos National Lab's MCNP (Lab, 2008) software is widely accepted and respected among nuclear engineers and scientists for determining neutron multiplication factors, reaction rates and for benchmarking criticality calculations (INL NEA/NSC DOC(95)03, 2009). Comparison of moments with Attila is important also because it is a multi-group transport code where 30 energy groups were used in the reported calculations. Table 1 shows the energy groups in the Attila 30 group library.

Simplification of EDNDE for moment equation developments

The starting point for formulation of an expression for analytical moments is Eq. (1). Eq. (1) is solved over the entire fission spectrum; which is well approximated to be from 0 to 10 MeV (Lamarsh, 1966). This analysis assumes steady state so the time dependent term, $\frac{1}{v}\frac{\partial\phi(\vec{r},E)}{\partial t}$ is set equal to zero. The system is homogenous so the energy dependent cross-sections and diffusion coefficient depend on energy only. The EDNDE, after the assumptions are applied has the following form in Eq. (6).

$$-D(E)\nabla^2\phi(\vec{r},E)+\Sigma_t(E)\phi(\vec{r},E)=\int_0^\infty \Sigma_s(E\to \acute{E})\phi(\vec{r},\acute{E},t)d\acute{E}+\chi(E)\times\int_0^\infty \nu(\acute{E})\Sigma(\acute{E})\phi(\vec{r},\acute{E})d\acute{E} \quad (6)$$

The differential scattering cross-section $\Sigma_s(E'\to E)$, is defined so that integrating from 0 to ∞, the probability of scattering into E is unity and yields $\Sigma_s(E)$ as the result (Duderstadt and Hamilton, 1976). The entire population of neutrons is treated as one large energy group E, from 0 to 10 MeV. The two assumptions change Eq. (6) into Eq. (7). Eq. (3) looks like the one-speed theory equation (Duderstadt and Hamilton, 1976, p. 295), except this equation retains the energy dependence of the cross-sections over the range of interest, 0–10 MeV where an overall energy dependent function $F(E)$ will be derived for and then transformed into the moment form of the EDNDE.

$$-D(E)\nabla^2\phi(\vec{r},E)+\Sigma_a(E)\phi(\vec{r},E)=\nu(E)\Sigma_f(E)\phi(\vec{r},E) \quad (7)$$

Derivation of $F(E)$ for energy moments

An appropriate approximation to the energy dependency of the macroscopic cross-sections and the diffusion coefficient is vital for any flux calculation; so a set of functions and constants have been carefully chosen so the energy dependent functionality is retained as much as possible and allow an analytic solution to be found. The macroscopic cross-sections may generally be divided into three distinct regions: thermal, resonance and fast, and in this analysis the authors consider a 4th region called the transition region and it spans from 2300 eV to 0.9 MeV. The reason for this subdivision is explained in more detail below.

The $1/v$ or $1/E^{1/2}$ law is a good approximation to the thermal region of many isotopes and found to be mathematically viable in foil activation (Morry and Williams, 1972). The cross-section data referred to and in use for this paper is from the evaluated nuclear data files, ENDF information is found on the web at http://atom.kaeri.re.kr/ (Institute, 2000) and http://t2.lanl.gov/data/neutron7.html (Lab, 2000). The resonance region, a summation of Breit-Wigner single level resonance formulas will be used to generate a function for this region to capture the complicated energy dependence. The functional piece that dominates the Breit-Wigner formulas in general is the $\frac{\text{Constant}_1}{(E-E_r)^2+\text{Constant}_2}$ term (Lamarsh, 1966, pp. 43–64). The transition to the fast region of the cross-sections generally has a $1/E$ drop off rate (Weinberg and Wigner, 1958, p. 57), and the fast region (0.1–10 MeV) has a $1/E^{5/2}$ with some broad resonances, which makes the fast region appear somewhat like a series of stair steps for ^{235}U $\Sigma_f(E)$.

It is very difficult to fit an analytic function to the resonance region, and the number of resonance peaks makes writing a function for each peak even more daunting, but with patience a single level Breit-Wigner can be written for each peak and has been for this work. A summation of these single level Breit-Wigner resonance functions was assembled to provide a functional form, that when integrated over the function would provide correct values when compared to the resonance values from *The Chart of the Nuclides and Isotopes 16th Edition* (Lockheed Martin/Knolls Atomic Power Laboratory, 2002). The simple functional approximations for the energy dependent cross-sections are somewhat crude but "if we choose the group constants properly, even one-speed diffusion theory could give an accurate description of nuclear reactor behavior" (Duderstadt and Hamilton, 1976, p. 295).

The general functional relationships for $D(E)$, $\nu(E)$, $\Sigma_f(E)$, $\Sigma_T(E)$, $\Sigma_S(E)$ and $\Sigma_a(E)$ with energy are incorporated into one function

of energy $F(E)$. The first step is to put all of the energy dependent functions together as one function of energy, labeled $F(E)$, see Eq. (8). The second step is to take $F(E)$ (Eq. (9)) and determine the functional shapes of $F(E)$ by using the ENDF-VII values arranged the same as $F(E)$, called ENDF-$F(E)$. This work only shows curve fits of $F(E)$ for 100% ^{235}U. The third step is to curve fit ENDF-$F(E)$ with the appropriate function fit for the different energy ranges. The result of the curve fit of ENDF-$F(E)$ is Eq. (16).

$$\nabla^2\phi(\vec{r},E)+\left(\frac{v(E)\Sigma_f(E)-\Sigma_a(E)}{D(E)}\right)\phi(\vec{r},E)=0 \tag{8}$$

$$F(E)=\frac{v(E)\Sigma(E)_f-\Sigma(E)_a}{D(E)}=3(v(E)\Sigma(E)_f-\Sigma(E)_a)(\Sigma(E)_t-\bar{\mu}\Sigma(E)_s) \tag{9}$$

It is assumed the total macroscopic cross-section, the transport cross-section, the function v(E) (the number of neutrons released in fission by an incident neutron of energy E), the neutron diffusion coefficient and the average angle of scatter are:

$$\Sigma(E)_t=\Sigma(E)_a+\Sigma(E)_s \tag{10}$$

$$\Sigma(E)_{i,tr}=\Sigma(E)_{i,t}-\bar{\mu}_i\Sigma(E)_{i,s} \tag{11}$$

$$D_i(E)=\frac{1}{3\Sigma(E)_{i,tr}}=\frac{1}{3\left(\Sigma(E)_{i,t}-\bar{\mu}i\Sigma(E)_{i,s}\right)} \tag{12}$$

$$v(E)=v_sE+\upsilon_{s0}\ \text{for}\ 0\leqslant E\leqslant 1\ \text{MeV} \tag{13}$$

$$v(E)=v_fE+\upsilon_{f0}\ \text{for}\ E>1\ \text{MeV} \tag{14}$$

$$\bar{\mu}_i=\frac{2}{3A} \tag{15}$$

A is the atomic mass number of isotope, (i). Eq. (15) is a decent approximation for the average angel of scatter for large atoms i.e. $A>16$. The function $v(E)$ is for ^{235}U where, $v_s=0.066$, $\upsilon_{s0}=2.432$, $v_f=0.15$, and $\upsilon_{f0}=2.349$ (Duderstadt and Hamilton, 1976, p. 61) if the energy variable is in units of MeV. The result of the function fit of ENDF-$F(E)$ is Eq. (16). Figs. 1–5 show comparisons of Eq. (16) with the ENDF-$F(E)$.

Fig. 1 shows the thermal region from 1E−5 eV to 1 eV on a log-log plot. The first term in Eq. (16) is the dominate feature in Fig. 1. The first resonance the $F(E)$ of pure ^{235}U is also seen in Fig. 1. Figs. 2–5 are not put on a log–log plots to point out the negative regions that show up from $v(E)\Sigma(E)_f-\Sigma(E)_a$ term in $F(E)$, where the absorption cross-section is greater than the product of $v(E)\Sigma(\mathrm{E})_f$.

Fig. 4 shows a comparison of ENDF-$F(E)$ to Eq. (16) for ^{235}U in the energy range of 895–1000 eV to show the difference between the two and how the "tails" of the resonance peaks overlap. Eq. (16) is not as sharp as the ENDF-$F(E)$ in the overlap spaces between each resonance peak.

Some of the minor peaks throughout the resonance region were not modeled i.e. peak height is less than 0.2 cm^{-2} (see Fig. 4). The reason for doing this is because the resonance integral value from *The Chart of the Nuclides and Isotopes 16th Edition* matched the resonance integral value from Eq. (16).

Fig. 5 shows the end of the resonance region and the beginning of the transition region.

Fig. 6 shows the transition region and the fast region up to 10 MeV.

$$F(E)=\frac{Rp_0}{E}+\sum_{l=1}^{N}\frac{Rp_l}{(E-Er_l)^2+w_l}+\sum_{m=1}^{N_{TRANS}}\frac{Rp_m\cdot(v_sE+\upsilon_{s0})_{2300\ \text{eV to 1 MeV}}}{(E-Er_m)^2+w_m}+\sum_{n=1}^{N_{FAST}}\frac{Rp_n\cdot(v_fE+\upsilon_{f0})_{E>1\ \text{MeV}}}{(E-Er_n)^4+w_n\cdot E} \tag{16}$$

The constants from Eq. (16) are: $Rp_0[=]\frac{Energy}{cm^2}$, $Rp'_{l,m}s[=]\frac{Energy^2}{cm^2}$, $Er'_{l,m,n}s[=]Energy$, $w'_{l,m}s[=]Energy^2$, $Rp'_ns[=]\frac{Energy^4}{cm^2}$, $w'_ns[=]Energy^3$, v_s & $v_f[=]\frac{neutrons}{Energy}$ and υ_{s0} & $\upsilon_{f0}[=]neutrons$, where N, N_{TRANS} and N_{FAST} are the number of terms included in each sum with indices l, m and n. The $Rp'_{l,m}s$ can be positive or negative because in some energy ranges $(-\Sigma(E)_a)$ is greater than in $(v(E)\Sigma(E)_f)$ Eq. (9). The data for each constant is in Appendix A. A 774 individual terms, $\left(\frac{Rp_l}{(E-Er_l)^2+w_l}\right)$ are accounted for in the first summation, 104 terms $\left(\frac{Rp_m\cdot(v_sE+\upsilon_{s0})_{2300\ \text{eV to 1 MeV}}}{(E-Er_m)^2+w_m}\right)$ in the second summation and nine individual terms $\left(\frac{Rp_n\cdot(v_fE+\upsilon_{f0})_{E>1\ \text{MeV}}}{(E-Er_n)^4+w_n\cdot E}\right)$ are accounted for in the third summation of Eq. (16).

The first term $\frac{Rp_0}{E}$ and the first summation term $\sum_{l=1}^{N}\frac{Rp_l}{(E-Er_l)^2+w_l}$ in Eq. (16) were observable by visual inspection of the ENDF-$F(E)$ plot. The first term comes from the $1/v$ portions of the cross-sections multiplied together and the first summation term captured ENFD-$F(E)$ in the energy range of 1–2250 eV. This range remained visually similar to the resonance region of ^{235}U $\Sigma(E)_t$ except for the few negative regions and the height and width of the each resonance peak which is specific to ENDF-$F(E)$ resonance peaks. The height and width of each ENDF-$F(E)$ peak can be matched by Eq. (16) by adjusting Rp_l and w_l respectively.

The second and third summation terms in Eq. (16) account for the linear effect of $v(E)$ on $F(E)$. The first and second terms of Eq. (16) are not affected by $v(E)$ because the slope is so small, just

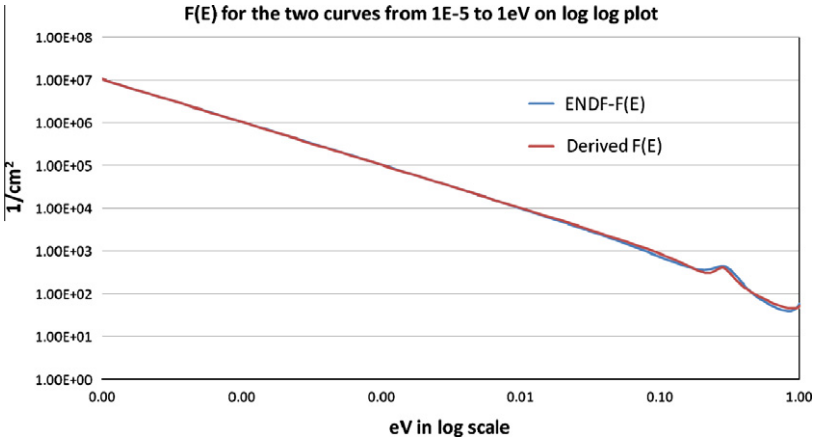

Fig. 1. Log–log plot of $F(E)$ from 1E−5 eV to 1 eV.

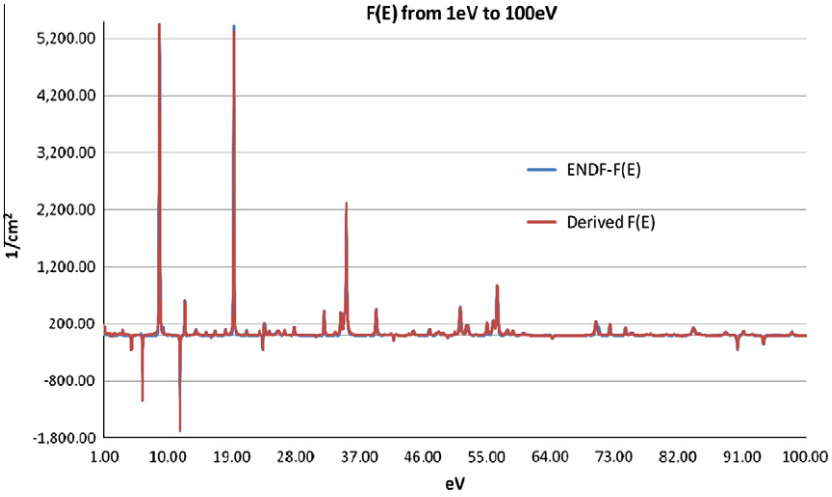

Fig. 2. Plot of $F(E)$ from 1 eV to 100 eV.

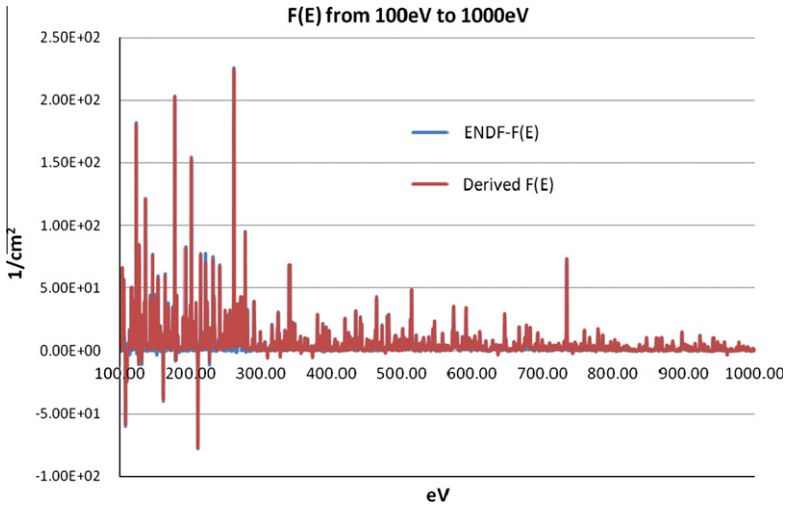

Fig. 3. Plot of $F(E)$ from 100 eV to 1000 eV.

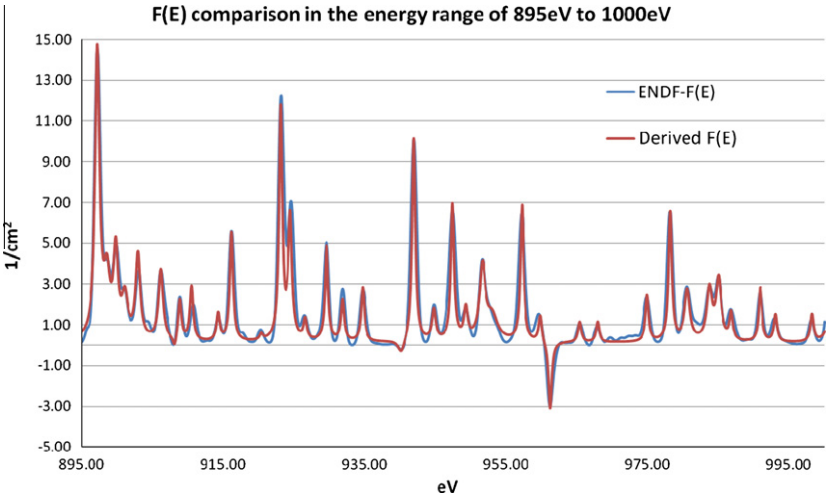

Fig. 4. $F(E)$ for pure ^{235}U from 895 eV to 1000 eV shows a closer view of the comparison of the two $F(E)$ functions.

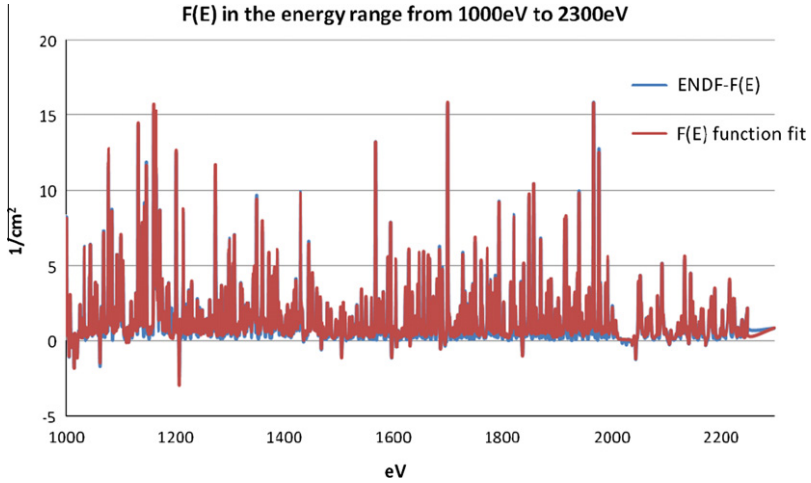

Fig. 5. Comparison plot of the derived $F(E)$ to the ENDF-$F(E)$ in the energy range of 100–2300 eV, the end of the resonance region.

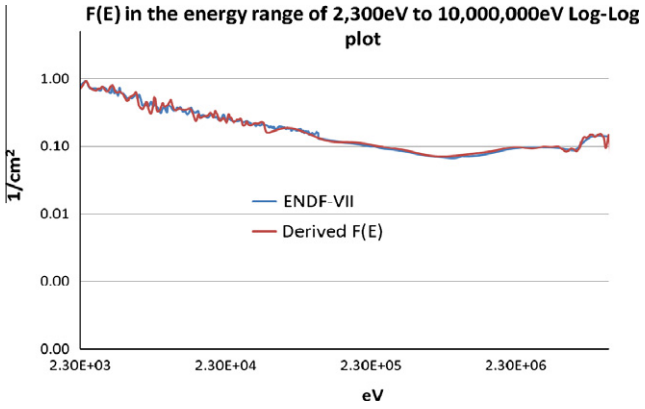

Fig. 6. Comparison of the two $F(E)$ functions from 2300 eV to 10 MeV.

the constant affects $F(E)$ and it is absorbed into Rp_0 and the $Rp_i's$. The slope of $\nu(E)$ does not change the value of $\nu(E)$ until roughly 46 keV and only from 2.43 to 2.44. It is included in the energy range at 2300 eV because of the shape of ENDF-$F(E)$ from 2300 eV to 0.9 MeV is a rough $1/E$ function, which $\frac{Rp_m\cdot(\nu_s E+\upsilon_{s0})_{2300\ eV\ to\ 1\ MeV}}{(E-Er_m)^2+w_m}$ is approximately a $1/E$ function. A summation of these terms $\frac{Rp_m\cdot(\nu_s E+\upsilon_{s0})_{2300\ eV\ to\ 1\ MeV}}{(E-Er_m)^2+w_m}$ provided a few useful qualities to fit the ENDF-$F(E)$ from 2300 eV to 0.9 MeV. The first is an ability to shift a $1/E$ function to this energy range at various places without the sharp discontinuity from these two $\frac{1}{(E-Er_m)}$ or $\frac{(\nu_s E+\upsilon_{s0})}{(E-Er_m)}$ functions or any similar function with an odd order in the denominator i.e. a term $\frac{1}{(E-Er_m)^{2n+1}}$ where $n = 0\ldots\infty$. The second reason this function is chosen is because it produced a smooth curve (see Fig. 6 from 0.1 MeV to 0.9 MeV) with a long forward tail which is the $1/E$ shape desired in this region without the sharp discontinuity. The third reason for this function is, small resonance peaks are in this energy range. The small peaks could be modeled with this function because it can be easily tuned by adjusting Rp_m and w_m to have a peak at the resonance energy Er^m.

The energy range 0.9–10 MeV yielded a different shape. In this energy range ENDF-$F(E)$ increased in a stair step shape (broad resonance) similar to the ^{235}U fission cross-section shape from 0.9 to 10 MeV. The slope of $\nu(E)$ in this energy range is larger and the effect from this linear function is greater. The term inside the third summation, $\frac{Rp_n\cdot(\nu_f E+\upsilon_{f0})_{E>1\ MeV}}{(E-Er_n)^4+w_n\cdot E}$ is used for similar reasons already mentioned: a smooth curve without sharp discontinuities (no odd ordered denominators), an ability to add an increase or "peak" at a specific energy (Er_n). The denominator $((E-Er_n)^4+w_n\cdot E)$ allowed for a much broader peak and a sharper drop off creating the level stair effect that corresponds to the broad width of the peak. The $w_n\cdot E$ in the denominator along with the 4th order term $(E-Er_n)^4$ restricted any long forward or backward tail that is seen with this these denominator choices $((E-Er_n)^2+E\cdot w_n)$ and $((E-Er_m)^2+w_m)$. The elimination of the long tails in this energy region was necessary to get the correct overlap between resonances; the other function choices investigated could not provide this effect in this energy region and consequently did not match the ENDF-$F(E)$.

These functions included into Eq. (16) allowed for analytic analysis and the development of analytic moments to be created.

Derivation of energy dependent neutron moments

The set of analytical energy dependent neutron moments are found from transforming Eq. (8) with the definition of a raw moment. The mathematical definition of a raw moment is $\boldsymbol{m_k} = \int_0^\infty E^k\boldsymbol{\phi}(\vec{\mathbf{r}},\mathbf{E})\mathbf{dE}$ where $k = 0, 1, 2, 3, \ldots, N$ (Casella and Berger, 2002) and N is the total number of moments desired. Transformation of Eq. (8) into moment form requires placing $F(E)$ into Eq. (8), multiply by, E^k then apply the definition of a moment i.e. integrate from 0 to infinity; the result is Eq. (17). The constant B^2_{Ek} in Eq. (17) is based on the diffusion boundary conditions that must be satisfied and is explained in the neutron diffusion boundary section of this paper.

$$\int_0^\infty \nabla^2\phi(\vec{r},E)dE + \int_0^\infty E^kF(E)\phi(\vec{r},E)dE + \int_0^\infty E^kB^2_{Ek}\phi(\vec{r},E)dE = 0 \tag{17}$$

The Laplace operator in Eq. (17) depends only on position so it comes through the energy integral, recognize the moment definition for two of the terms in Eqs. (17) and (18) is the 1 dimensional EDNDE in moment form

$$\nabla^2 m_k + B^2_{Ek}\cdot m_k + \int_0^\infty E^kF(E)\phi(\vec{r},E)dE = 0 \tag{18}$$

This new partial-integro differential equation, Eq. (18) needs to be simplified further to solve analytically. The term $E^kF(E)$ can be simplified as follows.

$$E^k \cdot F(E) = Rp_0 E^{k-1} + \sum_{l=1}^{N_{resonance}} \frac{E^k \cdot Rp_i}{E^2 - 2Er_l E + Er_l^2 + w_l} + \sum_{m=1}^{N_{TRANS}} \frac{E^k \cdot Rp_m \cdot (v_s E + \upsilon_{s0})_{0.1\ \text{MeV to}\ 1\ \text{MeV}}}{(E - Er_m)^2 + w_m} + \sum_{n=1}^{N_{FAST}} \frac{E^k \cdot Rp_n \cdot (v_f E + \upsilon_{f0})_{E>1\ \text{MeV}}}{(E - Er_n)^4 + w_n \cdot E} \quad (19)$$

The summations can be broken down into the various kth components by polynomial long division; an example of polynomial long divisions $\frac{c_1 u^k}{b_1 u^2 + b_2 u^1 + b_3} = \frac{c_1}{b_1} u^{k-2} + \frac{c_1 b_2}{b_1^2} u^{k-3} + \frac{c_1 (b_2^2 - b_1)}{b_1^3} u^{k-4} + \frac{c_1 (b_2^3 - b_1 b_2)}{b_1^3} u^{k-5} + \cdots +$ higher order terms.

In general, $E^k \cdot F(E)$ can now be written as

$$E^k \cdot F(E) = C_{E1} E^{k-1} + C_{E2} E^{k-2} + C_{E3} E^{k-3} + C_{E4} E^{k-4} + C_{E5} E^{k-5} + \cdots + \text{higher order terms}$$

where the constants are shown below with the units associated with them

$$C_{E1} = Rp_0 + \sum_{m=1}^{N_{TRANS}} v_s Rp_m \quad (20)$$

$$C_{E2} = \sum_{l=1}^{N} Rp_l + \sum_{m=1}^{NR_{TRANS}} (2Rp_m v_s Er_m + Rp_m v_{s0}) \quad (21)$$

$$C_{E3} = \sum_{l=1}^{N} 2Rp_l Er_l + \sum_{m=1}^{NR_{TRANS}} \left(3Rp_m v_s Er_m^2 + 2Er_m Rp_m v_0 - Rp_m v_s w_m\right) + \sum_{n=1}^{NR_{FAST}} Rp_n v_f \quad (22)$$

$$C_{E4} = \sum_{l=1}^{N} \left(3Rp_l Er_l^2 - Rp_l w_l\right) + \sum_{m=1}^{N_{TRANS}} \left(4Rp_m v_s Er_m^3 + 3Rp_m Er_m^2 v_{s0} - 4Rp_m Er_m v_s w_m - Rp_m w_m v_{s0}\right) + \sum_{n=1}^{N_{FAST}} (4Rp_n Er_n v_f + Rp_n v_{f0}) \quad (23)$$

$$C_{E5} = \sum_{l=1}^{N} 4Rp_l Er_l^3 + \sum_{m=1}^{N_{TRANS}} \left(5Rp_m v_s Er_m^4 + 4Rp_m Er_m^3 v_{s0} - 10Rp_m Er_m^2 v_s w_m - 4Er_m Rp_m w_m v_{s0} + Rp_m v_s w_m^2\right) + \sum_{n=1}^{N_{FAST}} \left(10Rp_n v_f Er_n^2 + 4Rp_n Er_n v_{f0}\right) \quad (24)$$

The higher order moments (k > 5) can be derived from dividing $F(E)$ further, but the 5th energy moment is sufficient to show how the moments from MCNP and Attila compare to the derived neutron diffusion moments. It has been shown that five moments is enough to reconstruct a particle population (Marchisio et al., 2003), but for neutron fluxes that still needs to be researched and sorted out. Table 2 shows the constants that come from Eqs. (20)–(24).

Eq. (18) becomes Eq. (25) by recognizing the terms in moment form in the integral of $E^k \cdot F(E)$.

Table 2
List of the energy constants from polynomial long division of $F(E)$.

Constant	Value	Units
CE1	0.0615	MeV/cm^2
CE2	0.0842	MeV^2/cm^2
CE3	0.3551	MeV^3/cm^2
CE4	2.1254	MeV^4/cm^2
CE5	13.5917	MeV^5/cm^2

$$\nabla^2 m_k + B_{Ek}^2 m_k + C_{E1} m_{k-1} + C_{E2} m_{k-2} + C_{E3} m_{k-3} + C_{E4} m_{k-4} + C_{E5} m_{k-5} = 0 \quad (25)$$

Eq. (25) is a set of partial differential equations, PDEs where the total number of equations is N. This analysis set N to be 5. This set of PDE's can be turned into a set of ordinary differential equations (ODEs) by making the assumption that the moments only depend on 1-dimension, r in this case. Each individual ODE moment equation is shown below and the set of moments work together as a system of equations.

$$\nabla^2 m_0 + B_{E0}^2 m_0 = -C_{E1} m_{-1} - C_{E2} m_{-2} - C_{E3} m_{-3} - C_{E4} m_{-4} - C_{E5} m_{-5} \quad (26)$$
$$\nabla^2 m_1 + B_{E1}^2 m_1 = -C_{E1} m_0 - C_{E2} m_{-1} - C_{E3} m_{-2} - C_{E4} m_{-3} - C_{E5} m_{-4} \quad (27)$$
$$\nabla^2 m_2 + B_{E2}^2 m_2 = -C_{E1} m_1 - C_{E2} m_0 - C_{E3} m_{-1} - C_{E4} m_{-2} - C_{E5} m_{-3} \quad (28)$$
$$\nabla^2 m_3 + B_{E3}^2 m_3 = -C_{E1} m_2 - C_{E2} m_1 - C_{E3} m_0 - C_{E4} m_{-1} - C_{E5} m_{-2} \quad (29)$$
$$\nabla^2 m_4 + B_{E4}^2 m_4 = -C_{E1} m_3 - C_{E2} m_2 - C_{E3} m_1 - C_{E4} m_0 - C_{E5} m_{-1} \quad (30)$$
$$\nabla^2 m_5 + B_{E5}^2 m_5 = -C_{E1} m_4 - C_{E2} m_3 - C_{E3} m_2 - C_{E4} m_1 - C_{E5} m_0 \quad (31)$$

Solution to the raw moment set come from setting the negative moments i.e. $k = -1, -2, -3$, etc. equal to zero. The reason for this is these moments are not in the set defined for k; $k = 0, 1, 2, 3, \ldots, N$. The set of ODEs is now Eq. (32)

$$\nabla^2 m_0 + B_{E0}^2 m_0 = 0 \quad (32)$$
$$\nabla^2 m_1 + B_{E1}^2 m_1 = -C_{E1} m_0 \quad (33)$$
$$\nabla^2 m_2 + B_{E2}^2 m_2 = -C_{E1} m_1 - C_{E2} m_0 \quad (34)$$
$$\nabla^2 m_3 + B_{E3}^2 m_3 = -C_{E1} m_2 - C_{E2} m_1 - C_{E3} m_0 \quad (35)$$
$$\nabla^2 m_4 + B_{E4}^2 m_4 = -C_{E1} m_3 - C_{E2} m_2 - C_{E3} m_1 - C_{E4} m_0 \quad (36)$$
$$\nabla^2 m_5 + B_{E5}^2 m_5 = -C_{E1} m_4 - C_{E2} m_3 - C_{E3} m_2 - C_{E4} m_1 - C_{E5} m_0 \quad (37)$$

Each kth moment can now be solved analytically beginning with the 0th raw moment. The rest of the raw moments can be solved analytically with the method of undetermined coefficients (Edwards and Penney, 2001). The solution to Eq. (32) for a 1 dimensional case turns out to be mathematically the same as the solution to the one-speed diffusion equation, which is comforting because this matches expectations and the flux shape from MCNP and Attila. The particular and homogeneous solutions to the ODE set with the corresponding constants for the raw energy dependent neutron diffusion moments are listed below in Eqs. (38)–(58).

$$m_0 = a_0 \frac{\sin(B_{E0} \cdot r)}{r} \quad (38)$$
$$m1 = a_1 \frac{\sin(B_{E1} \cdot r)}{r} + b_1 \cdot r \cdot \cos(B_{E1} \cdot r) \quad (39)$$

where

$$b_1 = \frac{a_0 C_{E1}}{2B_{E1}} \quad (40)$$
$$m_2 = a_2 \frac{\sin(B_{E2} \cdot r)}{r} + b_2 \cos(B_{E2} \cdot r) + c_2 r \sin(B_{E2} \cdot r) \quad (41)$$

where

$$b_2 = \frac{a_1 C_{E1} + a_0 C_{E2} + 2c_2}{2B_{E2}} \tag{42}$$

$$c_2 = -\frac{b_1 C_{E1}}{4B_{E2}} \tag{43}$$

$$m_3 = a_3 \frac{\sin(B_{E3} \cdot r)}{r} + b_3 \cos(B_{E3} \cdot r) + c_3 r \sin(B_{E3} \cdot r) + d_3 r^2 \cos(B_{E3} \cdot r) \tag{44}$$

where

$$b_3 = \frac{a_2 C_{E1} + a_1 C_{E2} + a_0 C_{E3} + 2c_3}{2B_{E3}}, \tag{45}$$

$$c_3 = -\frac{b_2 C_{E1} + b_1 C_{E2} + 6d_3}{4B_{E3}} \tag{46}$$

$$d_3 = \frac{c_2 C_{E1}}{6B_{E3}} \tag{47}$$

$$m_4 = a_4 \frac{\sin(B_{E4} \cdot r)}{r} + b_4 \cos(B_{E4} \cdot r) + c_4 r \sin(B_{E4} \cdot r) + d_4 r^2 \times \cos(B_{E4} \cdot r) + e_4 r^3 \sin(B_{E4} \cdot r) \tag{48}$$

where

$$b_4 = \frac{a_3 C_{E1} + a_2 C_{E2} + a_1 C_{E3} + a_0 C_{E4} + 2c_4}{2B_{E4}}, \tag{49}$$

$$c_4 = -\frac{b_3 C_{E1} + b_2 C_{E2} + b_1 C_{E3} + 6d_4}{4B_{E4}}, \tag{50}$$

$$d_4 = \frac{c_3 C_{E1} + c_2 C_{E2} + 12e_4}{6B_{E4}} \tag{51}$$

$$e_4 = -\frac{d_3 C_{E1}}{8B_{E4}} \tag{52}$$

$$m_5 = a_5 \frac{\sin(B_{E5} \cdot r)}{r} + b_5 \cos(B_{E5} \cdot r) + c_5 r \sin(B_{E5} \cdot r) + d_5 r^2 \times \cos(B_{E5} \cdot r) + e_5 r^3 \sin(B_{E5} \cdot r) + f_5 r^4 \cos(B_{E5} \cdot r) \tag{53}$$

where

$$b_5 = \frac{a_4 C_{E1} + a_3 C_{E2} + a_2 C_{E3} + a_1 C_{E4} + a_0 C_{E5} + 2c_5}{2B_{E5}}, \tag{54}$$

$$c_5 = -\frac{b_4 C_{E1} + b_3 C_{E2} + b_2 C_{E3} + b_1 C_{E4} + 6d_5}{4B_{E5}}, \tag{55}$$

$$d_5 = \frac{c_4 C_{E1} + c_3 C_{E2} + c_2 C_{E3} + 12e_5}{6B_{E5}}, \tag{56}$$

$$e_5 = -\frac{d_4 C_{E1} + d_3 C_{E2} + 20f_5}{8B_{E5}} \tag{57}$$

$$f_5 = \frac{e_4 C_{E1}}{10B_{E5}} \tag{58}$$

The unknown coefficients of the raw moments, a_k's and B_{Ek}'s are determined from the two neutron diffusion theory boundary conditions, after they are put in moment form.

Neutron diffusion boundary conditions in energy moment form

The first boundary condition that must be satisfied, is that the flux must be finite everywhere so the moments must be finite everywhere also. This condition is enforced by setting the amplitude constants in the $C_k \cdot \cos(B_{Ek}r)/r$ terms (which come from the homogeneous portion of the solution for each moment) equal to zero. The reason C_k is set to zero is; as the radius approaches zero, $C_k * \cos(B_{Ek}r)/r$ approaches infinity, so the C_k's are set to zero.

The second boundary condition is that the flux is zero at the transport corrected extrapolated boundary. The transport corrected extrapolated boundary is, $\widetilde{R} = R + r_o$, and $r_o = 2.13 \cdot D(E)$ where r_o is the extrapolated correction distance. For 1-group or 1-speed theory, $D(E)$ is the diffusion value for one energy value i.e. a 1 MeV neutron traveling through ^{235}U, $D(1\text{ MeV}) \approx 1$ cm (Foster and Wright, 1977, p. 250). For the purposes of having the correct boundary for each moment, $D(E)$ needs to ensure that at the appropriate extrapolated distance in moment form the neutron flux is zero. The boundary condition is satisfied and represented by the following relationship $m_k(\widetilde{R}) = \int_0^\infty E^k \phi(r = \widetilde{R}_k, E) dE = 0$. The boundary condition at the extrapolated distance in moment form is $\int_0^\infty \widetilde{R} E^k \phi(\vec{r}, E) dE = \int_0^\infty R E^k \phi(\vec{r}, E) dE + 2.13 * \int_0^\infty E^k \phi(\vec{r}, E) D(E) \quad dE$. Simplify the moment form of the extrapolated distance with the approximation that since this treatment is only at the boundary so the position dependence can be separated out and R and $\widetilde{R}$ can be treated as constants. Divide by the raw moment definition $\left(\int_0^\infty E^k \phi(\vec{r}, E) dE\right)$ on each side of the expression and the spatial dependence $\phi(\vec{r})$ come through the integrals, $\widetilde{R} \frac{\phi(\vec{r}) \int_0^\infty E^k \phi(E) dE}{\phi(\vec{r}) \int_0^\infty E^k \phi(E) dE} = R \frac{\phi(\vec{r}) \int_0^\infty E^k \phi(E) dE}{\phi(\vec{r}) \int_0^\infty E^k \phi(E) dE} + 2.13 * \frac{\int_0^\infty E^k D(E) \phi(\vec{r}, E) dE}{\int_0^\infty E^k \phi(\vec{r}, E) dE}$ the result is Eq. (59).

$$\widetilde{R}_k = R + 2.13 \cdot \frac{\int_0^\infty E^k D(E) \phi(E) dE}{\int_0^\infty E^k \phi(E) dE} \tag{59}$$

Values $\widetilde{R}_k$ are found with the energy dependent diffusion coefficient, $\left(D_i(E) = \frac{1}{3\Sigma_{i,tr}} = \frac{1}{3(\Sigma_{i,t} - \mu_i \Sigma_{i,s})}\right)$ the ENDF values for the cross-sections and the assumption that $\phi(E)$ is represented by Eq. (60) from 1 eV to 10 MeV (Duderstadt and Hamilton, 1976, p. 330). Below 1 eV the neutron flux is assumed to be a Maxwell–Boltzmann distribution at some temperature T (298 K) (Duderstadt and Hamilton, 1976). Eq. (61) represents (ξ) the average increase in lethargy per collision (Lamarsh, 1966, pp. 175–176).

$$\phi(E) = \frac{S}{\xi \cdot \Sigma(E)_s \cdot E} \tag{60}$$

$$\xi = \frac{2}{A + \frac{2}{3}} \tag{61}$$

This method allowed the extrapolated boundary to found for each moment and maintain the entire energy range of interest in a nuclear reactor by numerically integrating (Chapra and Canale, 2002) $\frac{\int_0^\infty E^k D(E) \phi(E) dE}{\int_0^\infty E^k \phi(E) dE}$ from Eq. (58). In the case of the 100% ^{235}U sphere the extrapolated boundaries are displayed in Table 3.

For the second boundary condition to be true, either $a_k = b_k = c_k = d_k = e_k = f_k = 0$, the null answer or B_{Ek} for each moment must satisfy the boundary condition. For the 0th moment, B_{E0} satisfies the second boundary condition by taking on the value of $\frac{\pi}{R_o}$, just like one speed theory and a_0 the other unknown coefficient is found by, the power equation, Eq. (72) in the next section. The rest of the moments, $k = 1$–5, the 2nd boundary condition is satisfied as follows, see Eqs. (62)–(66).

Table 3
The extrapolated boundaries for moment 0–5.

$\widetilde{R}_0$	$\widetilde{R}_1$	$\widetilde{R}_2$	$\widetilde{R}_3$	$\widetilde{R}_4$	$\widetilde{R}_5$
10.24 cm	10.25 cm	10.37 cm	10.38 cm	10.40 cm	10.40 cm

Table 4
List of the Rp_l's, Er_l's and w_l's.

Rp_l's	Er_l's	w_l's	Rp_l's	Er_l's	w_l's	Rp_l's	Er_l's	w_l's
−1	0.206	8.00E−03	3.4	590.59	0.10	0.75	1308.00	0.11
0.5	0.2819	2.10E−03	0.4	594.94	0.05	0.2	1311.80	0.23
−70.25	0.25	5.50E−01	3	596.16	0.50	0.05	1315.05	0.20
9.521	8.78	1.75E−03	0.675	598.90	0.10	0.2	1317.07	0.20
−1.15	6.39	1.00E−03	0.35	600.30	0.10	0.1	1318.90	0.20
−0.55	4.85	2.00E−03	1	603.22	0.10	0.7	1320.87	0.20
0.175	1.12	1.50E−03	2	604.40	0.30	0.8	1323.30	0.25
−0.125	2.04	2.50E−03	0.3	608.46	0.10	0.3	1326.05	0.20
0.01	3.14	1.50E−03	1.45	610.21	0.10	0.4	1329.83	0.20
0.1025	3.60	1.50E−03	0.3	612.90	0.10	0.4	1332.23	0.20
−1.65	11.67	1.00E−03	0.3	615.43	0.10	0.8	1333.80	0.40
0.48	12.38	8.00E−04	0.3	616.89	0.10	0.2	1335.50	0.50
8	19.30	1.50E−03	0.725	619.02	0.10	0.5	1336.99	0.30
0.4	23.41	1.50E−03	0.2	626.60	0.10	0.25	1338.75	0.20
0.11	21.07	1.50E−03	0.75	628.99	0.10	1.2	1343.01	0.30
0.13	22.94	1.75E−03	0.3	630.80	0.10	4	1346.56	0.85
0.2	24.29	2.65E−03	0.3	631.69	0.10	0.9	1350.41	0.10
1	23.62	4.75E−03	0.4	633.64	0.10	0.35	1355.60	0.30
1.425	13.99	1.50E−02	0.4	635.41	0.10	0.65	1358.80	0.50
0.075	15.40	1.50E−03	−0.4	636.50	0.10	1.5	1360.37	0.20
−0.075	16.09	1.50E−03	0.7	639.14	0.20	0.6	1363.28	0.75
3.175	25.55	4.15E−02	0.7	641.17	0.20	0.6	1364.07	0.95
0.375	26.49	4.50E−03	2.9	644.96	0.10	0.4	1367.66	0.35
0.115	16.67	1.50E−03	0.8	646.65	0.10	2	1372.05	0.35
0.13	18.05	1.40E−03	0.025	648.83	0.02	0.05	1375.13	0.30
0.625	27.79	4.50E−03	0.1	653.07	0.10	0.4	1378.20	0.10
1.75	32.06	4.15E−03	0.35	656.40	0.30	0.35	1380.70	0.25
−0.15	30.89	5.15E−03	0.65	658.38	0.10	1.35	1382.10	0.30
0.25	33.55	5.15E−03	0.5	663.60	0.10	3.5	1387.60	0.60
1.675	34.38	4.50E−03	1.85	665.92	0.10	0.5	1390.26	0.25
15	35.18	6.50E−03	0.4	672.13	0.10	0.5	1393.80	0.35
1.75	34.87	7.50E−03	0.9	674.11	0.10	1	1395.30	0.80
3.15	39.40	7.00E−03	3.5	676.42	0.20	0.01	1396.16	0.15
−0.675	41.86	6.50E−03	8	678.07	0.60	0.3	1400.75	0.40
1	41.51	3.50E−02	1.75	681.79	0.10	0.3	1403.45	0.20
0.8	42.25	4.00E−02	0.15	683.82	0.10	0.5	1406.40	0.23
−0.3	42.70	3.00E−02	0.6	685.53	0.50	0.4	1410.50	0.22
−0.07	43.36	6.00E−03	0.45	689.12	0.10	0.4	1415.29	0.18
0.65	189.5	2.50E−02	0.4	690.45	0.10	0.55	1418.47	0.18
1.01	192.32	1.25E−02	2.75	692.75	0.20	0.65	1421.17	0.18
0.6	194.18	2.50E−02	0.3	696.87	0.10	0.275	1423.63	0.20
2.65	198.5	7.50E−02	0.8	699.10	0.10	0.28	1425.77	0.20
3.05	200.28	2.00E−02	0.3	702.55	0.10	0.5	1427.20	0.40
1	203.73	4.50E−02	0.3	703.83	0.10	1.5	1430.07	0.17
0.95	206.99	2.50E−02	4	709.88	0.70	1.525	1433.53	1.00
−1.65	209.6	2.10E−02	0.3	715.75	0.10	−0.2	1436.27	0.50
1.15	213.65	1.50E−02	0.3	717.13	0.10	0.2	1439.50	0.50
0.25	217.105	2.10E−02	0.3	718.90	0.10	0.1	1442.53	0.50
5	220.62	7.50E−02	0.3	719.92	0.10	1.575	1431.75	1.00
2.5	221.69	1.00E−01	0.5	721.59	0.10	1.25	1445.29	0.20
0.55	223.16	1.50E−02	0.6	723.53	0.20	0.85	1449.75	0.28
−0.255	226.32	2.10E−02	0.2	727.41	0.10	1.25	1451.81	0.30
0.65	226.74	3.50E−02	0.65	729.38	0.10	0.25	1454.09	0.30
0.65	229.09	6.50E−02	7.3	733.36	0.10	0.4	1456.41	0.40
3.2	231.45	4.50E−02	0.4	737.69	0.10	1	1459.68	0.30
1	232.89	2.50E−02	0.5	739.95	0.10	0.1	1463.74	0.40
1	233.83	6.50E−02	−0.65	741.74	0.28	0.95	1465.65	0.34
4.3	241.16	6.50E−02	0.6	745.35	0.10	−0.2	1467.57	0.20
0.75	245.44	6.50E−02	0.4	747.06	0.10	0.2	1469.52	0.20
0.75	247.91	6.50E−02	0.2	750.00	0.10	0.3	1472.37	0.40
2	248.94	6.50E−02	0.2	751.22	0.10	0.6	1479.7	0.25
4	253.5	1.50E−01	0.5	754.05	0.10	0.25	1483.01	0.25
2	255.95	6.50E−02	1.6	758.84	0.10	0.5	1486.02	0.25
0.55	259.92	6.50E−02	0.25	761.71	0.10	0.4	1494.8	0.30
14.5	261.65	6.50E−02	0.25	762.87	0.10	0.35	1498.06	0.30
1.25	266.35	3.50E−02	2.5	766.31	0.25	0.2	1500.95	0.30
1	268.2	9.50E−02	0.1	767.99	0.10	0.45	1503.3	0.20
3.5	270.01	8.50E−02	0.3	770.88	0.10	−0.3	1504.85	0.20
3.5	272.78	8.50E−02	0.35	772.63	0.10	0.5	1507.83	0.20
1.85	276.78	2.00E−02	1.5	778.46	0.10	0.025	1509.93	0.20
2	279.84	6.50E−02	2.35	779.41	0.20	0.35	1511.82	0.20
0.35	287.38	4.50E−02	0.25	782.38	0.10	0.3	1520.17	0.20
4	289.46	1.00E−01	1.2	785.3	0.10	0.45	1524.9	0.30
0.15	295.93	4.00E−02	0.3	790.32	0.10	0.2	1527.7	0.30

(*continued on next page*)

Table 4 (*continued*)

Rp_i's	Er_i's	w_i's	Rp_i's	Er_i's	w_i's	Rp_i's	Er_i's	w_i's
0.075	298.5	5.25E−03	0.3	792.61	0.10	0.25	1530.29	0.30
0.15	302.79	4.00E−02	0.5	795.5	0.08	0.65	1533.32	0.30
0.2	43.96	7.50E−03	0.3	796.28	0.08	0.15	1535.37	0.30
1	44.61	1.25E−02	1.65	801.33	0.20	0.15	1538.43	0.15
1	46.93	9.75E−03	0.9	806.01	0.20	0.5	1541.51	0.15
1	47.93	2.60E−02	1.6	806.95	0.40	0.1	1546.39	0.50
1.4	48.3	2.60E−02	0.05	810.11	0.08	1	1549.41	0.35
0.2	48.80	5.50E−03	0.55	812.757	0.30	0.05	1551.61	0.20
0.255	49.43	5.50E−03	1.45	815.11	0.50	0.2	1553.94	0.30
0.3	50.48	5.50E−03	0.25	817.9	0.10	0.7	1559.77	0.25
3.65	51.26	7.50E−03	0.65	818.9	0.20	1.5	1567.81	0.12
3.5	52.21	2.00E−02	0.15	821.86	0.08	0.2	1570.94	0.20
1.58	55.04	7.50E−03	0.05	823.55	0.08	0.5	1573.8	0.20
6	55.88	2.50E−02	0.05	825.51	0.08	0.5	1575.55	0.75
6.45	56.48	7.50E−03	0.05	828.5	0.08	0.7	1579.2	0.30
1.7	57.95	2.00E−02	0.05	830.13	0.08	0.9	1581.44	0.30
0.55	58.66	7.50E−03	0.675	837.15	0.15	0.3	1587.27	0.90
0.85	60.18	2.00E−02	0.9	843.03	0.30	1.075	1589.71	0.20
−0.55	64.30	1.00E−02	1.5	847.2	0.15	1.575	1594.4	0.20
6	70.43	2.50E−02	0.1	851.29	0.15	−0.7	1596.31	0.40
0.95	72.36	5.00E−03	0.05	852.8	0.10	0.4	1598.54	0.50
0.65	74.54	5.00E−03	0.05	854.9	0.10	0.05	1600.54	0.50
1.25	75.49	3.00E−02	0.1	858.3	0.10	1.35	1604.4	0.25
−0.2	82.63	1.00E−02	0.7	861.36	0.08	−0.35	1606.4	0.40
5.15	84.15	4.00E−02	0.7	862.68	0.08	0.1	1609.25	0.20
0.65	84.99	3.00E−02	0.3	866.17	0.08	0.05	1612.53	0.20
1.6	88.75	3.00E−02	0.75	867.95	0.08	0.4	1616.18	0.60
−1.5	94.07	1.00E−02	0.025	871.5	0.08	0.2	1619.7	0.30
−2.55	90.35	1.00E−02	0.3	875.45	0.08	0.5	1622.2	0.15
0.5	89.77	3.50E−02	0.4	879.06	0.15	0.875	1628.13	0.15
2.65	91.24	3.50E−02	0.4	881	0.15	−0.1	1630.18	0.15
0.75	92.52	3.50E−02	0.5	883.81	0.08	0.55	1633.9	0.18
1.5	98.07	2.50E−02	0.95	884.94	0.30	0.2	1637.74	0.60
0.35	77.5	2.00E−02	0.1	886.84	0.30	0.45	1639.98	0.30
0.5	78.08	2.00E−02	0.1	892.69	0.08	0.62	1644.06	0.18
0.5	80.34	3.00E−02	−0.4	803.71	0.40	1	1647	0.18
0.5	81.42	3.00E−02	2.05	897.16	0.15	0.3	1650	0.25
0.65	102.91	1.00E−02	0.6	899.73	0.15	0.1	1652.5	0.50
0.55	105.21	1.00E−02	0.6	902.9	0.15	0.875	1655.64	0.15
−0.6	107.62	1.00E−02	0.5	906.09	0.15	1.2	1663.81	0.23
0.25	305.06	4.00E−02	0.15	908.82	0.08	1.2	1665.9	0.24
−0.25	308.95	4.00E−02	0.2	910.46	0.08	0.3	1671.24	0.24
0.1	312.52	4.00E−02	−0.05	908.1	0.09	0.4	1672.77	0.15
0.075	313.55	4.00E−02	0.1	914.25	0.08	0.375	1675.12	0.20
1.25	315.35	6.50E−02	0.4	916.1	0.08	0.685	1679.47	0.18
0.25	319.66	4.00E−02	0.02	920.34	0.07	0.685	1681.55	0.22
1	323.56	6.50E−02	0.85	923.05	0.08	1.25	1683.76	0.21
1.5	324.28	5.50E−02	0.6	924.42	0.10	−0.475	1685.43	0.40
1	325.97	8.50E−02	0.075	926.53	0.08	0.7	1690.01	0.15
−0.25	327.21	4.00E−02	0.35	929.56	0.08	−0.2	1695	0.40
0.25	329.27	4.00E−02	0.15	931.84	0.08	2.35	1699.63	0.15
0.1	330.6	4.00E−02	0.2	934.66	0.08	0.4	1701.95	0.35
0.3	332.44	4.00E−02	−0.2	940.09	0.30	0.25	1702.96	0.25
0.25	334.05	1.65E−02	0.75	941.91	0.08	0.075	1706.86	0.25
0.225	336.63	1.65E−02	0.15	944.72	0.10	0.17	1709.31	0.25
0.1	338.71	4.00E−02	0.5	947.39	0.08	0.3	1713.64	0.25
1.25	340.07	1.85E−02	0.15	949.25	0.10	0.4	1717.47	0.25
0.125	342.23	4.00E−02	0.9	951.6	0.25	0.1	1720.12	0.30
0.325	343.95	1.50E−02	0.5	957.19	0.08	0.65	1722.5	0.30
0.31	346.98	1.50E−02	0.1	959.78	0.08	1.25	1726.36	0.23
0.1	349.37	4.00E−02	−0.25	961.17	0.08	0.65	1731.66	0.22
0.1	350.73	4.00E−02	0.075	965.36	0.08	0.65	1735.01	0.30
0.2	351.65	4.00E−02	0.075	967.88	0.08	0.2	1738.22	0.40
0.25	353.14	3.75E−02	0.17	974.9	0.08	0.6	1741.22	0.20
0.25	355.33	2.25E−02	0.475	978.14	0.08	0.7	1745.56	0.20
−0.12	356.06	4.00E−02	0.5	980.58	0.20	1.32	1749.6	0.20
0.1	359.66	4.00E−02	0.5	983.69	0.20	0.6	1751.58	0.50
0.1	360.51	4.00E−02	0.6	984.99	0.20	0.2	1755.03	0.35
0.275	361.6	3.00E−02	0.1	986.79	0.08	1	1760.23	0.20
0.7	365.28	8.00E−02	0.2	990.9	0.08	1	1762.1	0.50
0.1	370.38	4.00E−02	0.1	993.05	0.08	1.2	1771.82	0.20
0.1	371.31	4.00E−02	0.1	998.23	0.08	0.3	1774.44	0.15
−0.25	372.6	4.00E−02	0.7	898.5	0.25	0.8	1777.28	0.25
0.125	373.14	4.00E−02	0.5	901	0.25	0.9	1779.3	0.25
0.165	377.72	4.00E−02	1	953	0.85	0.9	1783.3	0.30

Table 4 (*continued*)

Rp_i's	Er_i's	w_i's	Rp_i's	Er_i's	w_i's	Rp_i's	Er_i's	w_i's
1	379.81	3.50E−02	0.6	1001.05	0.08	1	1788.37	0.25
0.6	383.34	5.35E−02	0.1	1004.42	0.08	0.1	1791.43	0.20
0.85	387.48	4.00E−02	−0.1	1005.67	0.08	2	1794.88	0.22
−0.5	109.79	2.00E−02	0.225	1007.5	0.08	0.175	1799.53	0.40
0.15	113.55	1.00E−02	0.03	1010.49	0.08	0.5	1803.07	0.20
0.75	115.94	1.50E−02	−0.1	1011.24	0.15	0.3	1808.12	1.00
1.75	118.23	4.50E−02	−0.15	1014.7	0.08	0.75	1815.7	0.20
1.25	121.92	7.00E−03	0.12	1015.91	0.25	0.5	1819.56	0.30
0.45	124.75	3.50E−02	−0.1	1017.62	0.08	2	1821.9	0.25
5.5	125.98	7.50E−02	0.05	1019.08	0.25	0.4	1825.24	0.20
2	126.35	5.00E−02	−0.1	1020.1	0.08	0.3	1829.04	0.50
−0.5	125.5	1.50E−02	0.1	1022.77	0.25	0.3	1830.74	0.75
−0.15	129.9	1.50E−02	0.175	1025.15	0.08	0.75	1835	0.20
0.25	128.05	2.00E−02	0.1	1030.53	0.08	−0.8	1837.8	0.50
1	131.29	4.00E−02	0.455	1033.27	0.08	1.55	1839.86	0.30
1.4	132.08	7.50E−02	0.05	1036.5	0.08	0.2	1843.17	0.50
1.1	132.7	5.00E−02	1.1	1043.75	0.30	4	1849.52	0.42
0.35	133.54	1.00E−02	0.825	1044.82	0.15	2.05	1857.55	0.20
3	135.25	2.50E−02	0.2	1049.66	0.08	0	1860.42	0.10
1.2	141.99	3.00E−02	0.9	1053.64	0.25	0.6	1863.3	0.30
0.75	145.54	1.00E−02	0.85	1056.08	0.25	0.3	1865.9	0.30
0.3	147.26	2.00E−02	0.15	1059.8	0.15	0.1	1868.3	0.30
1.2	149.06	3.00E−02	−0.1375	1061.87	0.08	1.15	1871.36	0.18
0.35	149.88	3.00E−02	0.6	1064.03	0.30	0.295	1875.05	0.20
0.285	153.38	5.00E−03	1.25	1068.19	0.18	0.5	1877.8	0.60
0.25	154.83	3.00E−02	0.05	1071.4	0.06	0.9	1881.95	0.30
0.35	156.75	2.00E−02	0.05	1074.62	0.10	0.75	1885.1	0.20
0.55	158.51	5.00E−02	2.15	1076.83	0.23	1.2	1889.61	0.30
0.55	159.12	5.00E−02	2.1	1077.74	0.20	0	1893.33	0.50
−0.8	160.94	2.00E−02	0.1	1080.06	0.08	0.4	1897.04	0.20
1.45	163.6	2.50E−02	1	1082.56	0.30	0.55	1902.6	0.20
1.55	166.25	7.50E−02	0.6	1084.2	0.08	0.45	1906.65	0.30
0.85	168.02	2.50E−02	0.05	1086.75	0.08	0.2	1910.42	0.30
0.35	169.33	2.50E−02	0.8	1089.92	0.40	2.25	1915.5	0.30
2.75	174.48	8.50E−02	0.4	1093.28	0.08	2.3	1917.54	0.30
0.45	176.54	2.50E−02	0.4	1095.59	0.23	0.95	1922.7	0.30
3.75	177.54	1.87E−02	0.75	1097.5	0.30	0.7	1924.5	0.40
−0.3	178.54	2.50E−02	2	1100.16	0.30	0.6	1930.37	0.30
−0.25	179.42	2.50E−02	1.5	1103.44	0.30	0.6	1933.32	0.20
1.05	180.31	2.50E−02	0.075	1108.42	0.20	1.25	1937.95	0.30
0.65	181.99	6.50E−02	−0.04	1110	0.10	1.85	1940.64	0.20
0.7	392.17	4.00E−02	0.07	1111.2	0.10	1	1945.2	0.60
0.1	356.7	4.00E−02	−0.1	1113.62	0.30	0.4	1952.2	0.35
0.5	396.55	3.25E−02	0.1	1116.08	0.15	0.85	1955.3	0.30
0.1	402.18	3.50E−02	0.75	1118.3	0.30	1	1960.3	0.30
1.752	405.1	2.00E−01	0.35	1123.6	0.30	0.7	1963.67	0.30
0.3	408.45	5.00E−02	0.535	1126.11	0.50	3.2	1967.8	0.21
0.1	414.37	4.00E−02	0.425	1128.2	0.15	0.5	1972.71	1.00
0.25	415.34	5.00E−02	1.345	1132.3	0.10	2.2	1977.16	0.18
0.75	418.26	3.00E−02	0.15	1134.39	0.20	0.9	1979.7	0.28
0.35	419.83	4.00E−02	0.6	1136.48	0.35	0.2	1983.8	0.80
0.535	423.25	4.00E−02	2.645	1139.08	0.35	0.3	1985.8	0.50
0.425	425.46	4.00E−02	0.85	1143.43	0.10	1.1	1989.29	0.30
0.215	427.42	4.00E−02	1.7	1146.66	0.15	1.1	1993.6	0.20
0.15	428.83	4.00E−02	0.075	1149.9	0.15	0.3	1997.85	0.70
0.75	430.66	9.00E−02	0.1	1152.79	0.20	0.6	1999.84	0.70
1.2	433.81	4.00E−02	0.5	1156.1	1.00	1	2002.45	0.50
2	434.88	2.00E−01	1.1	1159.65	0.08	0.3	2006.36	0.50
0.3	439.14	4.00E−02	1.9	1161.5	0.28	0.6	2008.22	0.50
1.025	440.4	4.00E−02	3.8	1163.3	0.28	0.1	2010.9	0.30
0.81	442.26	4.00E−02	2.5	1165.23	0.25	−0.18	2037.9	0.50
0.1	448.5	4.00E−02	1	1167.55	0.20	−0.27	2045.17	0.20
0.85	449.94	1.00E−01	0.6	1170.27	0.10	0.1	2042.43	0.40
0.3	453.7	4.00E−02	0.8	1172	0.10	0.75	2050.17	0.20
0.7	458.7	1.00E−01	0.5	1174	0.20	0.7	2053.18	0.19
1.5	462.02	1.00E−01	0.75	1175.99	0.20	2	2054.84	0.90
3.5	463.8	8.50E−02	0.1	1178.6	0.25	0.2	2058.85	0.60
0.05	466.53	2.00E−02	0.5	1180.7	0.30	0.4	2063.75	0.30
0.6	468.93	1.00E−01	1	1184.41	0.30	0.5	2067.31	0.35
0.75	471.77	4.00E−02	0.9	1187.46	0.25	0.4	2069.75	0.35
−0.1	476.53	4.00E−02	0.1	1190.1	0.08	1	2072.10	0.50
0.1	477.16	4.00E−02	0.1	1192.67	0.08	0.2	2081.23	1.00
1	479.23	3.80E−02	0.1	1194.18	0.08	0.75	2085.12	0.26
1.05	481.33	3.80E−02	0.4	1197.20	0.25	1	2090.43	0.60
0.2	483.51	5.50E−02	1.25	1200.80	0.10	2	2093.07	0.42

(*continued on next page*)

Table 4 (*continued*)

Rp_l's	Er_l's	w_l's	Rp_l's	Er_l's	w_l's	Rp_l's	Er_l's	w_l's
0.1	485.29	4.00E−02	0.3	1204.56	0.30	0.5	2095.29	0.40
0.2	487.1	4.75E−02	−0.35	1206.15	0.10	1	2099.65	1.65
0.4	489.46	5.50E−02	0.5	1207.49	0.35	−0.5	2106.22	1.25
0.6	490.47	5.50E−02	3	1214.20	0.35	0.5	2108.78	0.80
0.425	495.64	5.00E−02	0.175	1216.10	0.25	0.2	2118.20	0.70
1.65	500.28	1.00E−01	0.4	1220.19	0.20	0.75	2121.42	0.70
2	502.1	2.50E−01	0.6	1224.59	0.20	0.3	2124.65	0.50
2	503.36	2.50E−01	0.25	1225.88	0.20	0.75	2129.05	0.50
0.4	506.01	1.00E−01	0.75	1229.70	0.20	2.75	2134.61	0.50
0.4	507.89	5.00E−02	0.5	1232.86	0.40	0.2	2137.75	0.35
2.4	511.40	1.00E−01	0.4	1235.60	0.40	−0.35	2141.90	0.70
2.35	513.16	5.00E−02	0.1	1237.34	0.10	1.75	2145.14	0.40
1.2	519.76	1.00E−01	0.5	1239.65	0.20	0.85	2148.50	0.35
0.2	524.29	5.00E−02	0.75	1243.20	0.40	0.6	2153.21	0.40
0.3	528.03	5.00E−02	0.75	1248.20	0.40	0.4	2160.80	0.35
4	530.51	4.00E−01	0.3	1251.71	0.25	1	2164.15	0.50
0.3	535.33	9.00E−02	0.3	1254.05	0.25	0.7	2168.27	0.35
1	537.81	1.00E−01	0.2	1255.81	0.25	−0.45	2172.90	1.00
0.1	539.84	5.00E−02	0.45	1258.17	0.35	0.7	2179.37	0.40
0.23	542.15	5.00E−02	0.65	1263.12	0.25	4	2183.35	1.40
0.85	543.81	5.00E−02	0.15	1267.02	0.20	0.75	2189.31	0.23
1.15	546.19	5.00E−02	0.4	1268.31	0.30	0.1	2196.33	1.00
0.625	551.91	1.50E−01	0.4	1270.00	0.30	0.45	2199.99	0.75
2	557.77	1.50E−01	1.15	1272.95	0.10	0.75	2202.80	0.40
0.4	561.01	1.00E−01	0.25	1278.46	0.10	0.25	2207.17	0.70
0.3	564.73	9.00E−02	0.25	1280.37	0.10	4	2213.88	2.00
0.35	566.70	2.00E−01	0.35	1283.72	0.10	3.65	2216.99	1.00
0.75	570.98	5.00E−02	0.2	1287.50	0.50	1.15	2223.71	0.45
3	572.56	8.50E−02	0.3	1290.61	0.10	1.15	2226.61	0.45
2	575.83	2.00E−01	1	1291.89	0.80	0.3	2233.24	0.45
3.9	577.64	3.00E−01	1.375	1296.89	0.25	0.3	2236.21	0.75
0.05	579.60	2.00E−02	1.375	1298.63	0.23	1.2	2240.52	0.90
3	585.50	3.00E−01	0.1	1300.78	0.10	0.5	2247.90	0.35
0.3	587.50	5.00E−02	1	1305.59	0.21	0.2	2250.00	0.10

Table 5
List of the Rp_m's, Er_m's and w_m's.

Rp_m's	Er_m's	w_m's	Rp_m's	Er_m's	w_m's	Rp_m's	Er_m's	w_m's
2.50E−05	2.30E+03	8.00E+03	5.00E−06	8.00E+03	2.00E+04	1.00E−05	2.10E+04	1.60E+05
6.00E−05	2.50E+03	1.50E+04	5.00E−06	8.20E+03	2.00E+04	1.00E−05	2.21E+04	1.00E+05
1.50E−05	2.65E+03	8.50E+03	5.00E−06	8.40E+03	2.00E+04	1.00E−05	2.32E+04	2.60E+05
1.50E−05	2.90E+03	1.00E+04	5.00E−06	8.50E+03	2.00E+04	1.00E−05	2.37E+04	2.60E+05
1.50E−05	3.00E+03	1.00E+04	5.00E−06	8.70E+03	2.00E+04	1.00E−05	2.40E+04	2.60E+05
9.00E−06	3.15E+03	8.00E+03	5.00E−06	9.00E+03	2.00E+04	1.00E−05	2.42E+04	2.60E+05
2.00E−05	3.25E+03	1.00E+04	5.00E−06	9.15E+03	2.00E+04	1.00E−05	2.46E+04	5.00E+05
1.50E−05	3.50E+03	1.00E+04	5.00E−06	9.50E+03	2.00E+04	1.00E−05	2.50E+04	2.00E+05
1.50E−05	3.70E+03	1.00E+04	5.00E−06	9.60E+03	2.00E+04	1.00E−05	2.57E+04	3.00E+05
1.20E−05	3.80E+03	1.00E+04	7.00E−06	1.00E+04	5.00E+04	1.00E−05	2.62E+04	3.00E+05
8.00E−06	3.90E+03	1.00E+04	1.00E−04	1.04E+04	1.00E+06	1.00E−05	2.72E+04	3.00E+05
8.00E−06	4.00E+03	1.00E+04	1.00E−04	1.07E+04	1.00E+06	1.00E−05	2.75E+04	3.00E+05
8.00E−06	4.15E+03	1.00E+04	1.00E−04	1.09E+04	1.00E+06	1.00E−05	2.83E+04	3.00E+05
8.00E−06	4.25E+03	1.00E+04	5.00E−05	1.12E+04	1.00E+06	1.00E−05	2.88E+04	3.00E+05
8.00E−06	4.35E+03	1.00E+04	5.00E−05	1.17E+04	1.00E+06	1.00E−05	2.93E+04	3.00E+05
1.10E−05	4.50E+03	1.00E+04	5.00E−05	1.20E+04	1.00E+06	1.00E−05	3.00E+04	5.00E+05
8.00E−06	4.80E+03	1.00E+04	5.00E−05	1.24E+04	1.00E+06	1.00E−05	3.11E+04	5.00E+05
8.00E−06	5.00E+03	1.00E+04	5.00E−05	1.28E+04	1.00E+06	1.00E−05	3.18E+04	5.00E+05
8.00E−06	5.15E+03	1.00E+04	5.00E−05	1.31E+04	1.00E+06	1.00E−05	3.21E+04	5.00E+05
8.00E−06	5.35E+03	1.00E+04	5.00E−05	1.31E+04	1.00E+06	1.00E−05	3.28E+04	5.00E+05
8.00E−06	5.50E+03	1.00E+04	5.00E−05	1.33E+04	1.00E+06	1.00E−05	3.42E+04	5.00E+05
5.00E−06	5.60E+03	1.50E+04	5.00E−05	1.37E+04	1.00E+06	1.00E−05	3.50E+04	5.00E+05
5.00E−06	5.65E+03	1.50E+04	5.00E−06	1.43E+04	1.00E+06	1.00E−05	3.62E+04	5.00E+05
5.00E−06	5.80E+03	1.50E+04	5.00E−06	1.48E+04	7.00E+04	1.00E−05	3.70E+04	6.00E+05
5.00E−06	6.00E+03	1.50E+04	5.00E−06	1.50E+04	7.00E+04	1.00E−05	3.79E+04	6.00E+05
5.00E−06	6.15E+03	1.50E+04	5.00E−06	1.53E+04	7.00E+04	1.00E−05	3.91E+04	6.00E+05
5.00E−06	6.40E+03	1.50E+04	1.00E−05	1.60E+04	7.00E+04	1.00E−05	4.00E+04	6.00E+05
5.00E−06	6.50E+03	1.50E+04	1.00E−05	1.72E+04	7.00E+04	1.00E−05	4.10E+04	6.00E+05
5.00E−06	6.60E+03	1.50E+04	1.00E−05	1.79E+04	7.00E+04	1.00E−05	4.20E+04	6.00E+05
5.00E−06	6.75E+03	2.00E+04	7.50E−06	1.84E+04	7.00E+04	5.00E−02	5.00E+04	1.10E+09
5.00E−06	7.00E+03	2.00E+04	7.50E−06	1.89E+04	1.00E+05	5.55E−02	1.50E+05	1.05E+10
5.00E−06	7.25E+03	2.00E+04	7.50E−06	1.94E+04	7.00E+04	7.00E−02	3.00E+05	4.35E+10
5.00E−06	7.35E+03	1.00E+04	1.00E−05	1.98E+04	1.60E+05	1.22E−01	5.00E+05	4.85E+11
5.00E−06	7.50E+03	1.00E+04	1.00E−05	2.00E+04	1.60E+05	6.20E−01	9.00E+05	1.00E+12
5.00E−06	7.70E+03	2.00E+04	1.00E−05	2.05E+04	1.60E+05			

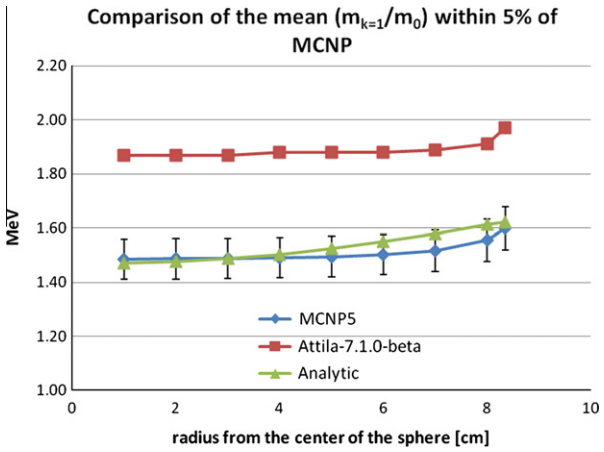

Fig. 7. Comparison plot of the mean energy for the GODIVA benchmark.

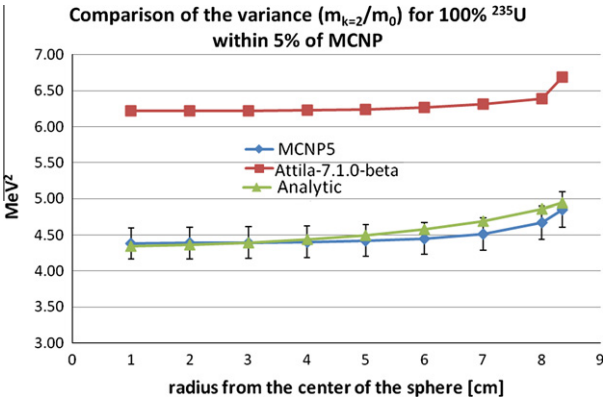

Fig. 8. Comparison plot of the variance of energy for the GODIVA benchmark.

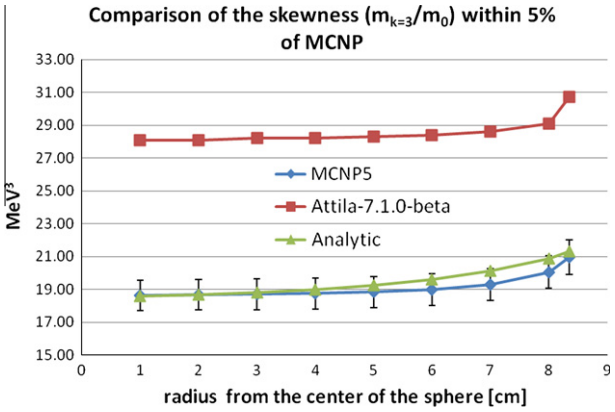

Fig. 9. Comparison plot of the skewness of energy for the GODIVA benchmark.

$$\frac{a_1}{\widetilde{R}_1}\sin(B_{E1}\cdot\widetilde{R}_1) = -b_1\cos(B_{E1}\cdot\widetilde{R}_1) \tag{62}$$

$$\left(\frac{a_2}{\widetilde{R}_2}+c_2\widetilde{R}_2\right)\sin(B_{E2}cdot\widetilde{R}_2) = -b_2\cos(B_{E2}\cdot\widetilde{R}_2) \tag{63}$$

$$\left(\frac{a_3}{\widetilde{R}_3}+c_3\widetilde{R}_3\right)\sin(B_{E3}\cdot\widetilde{R}_3) = -\left(b_3+d_3\widetilde{R}_3^2\right)\cos(B_{E3}\cdot\widetilde{R}_3) \tag{64}$$

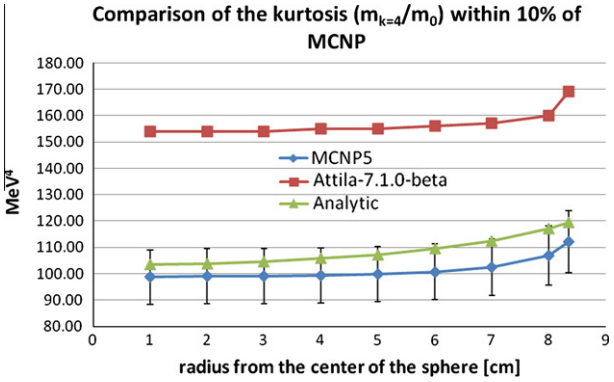

Fig. 10. Comparison plot of the kurtosis of energy for the GODIVA benchmark.

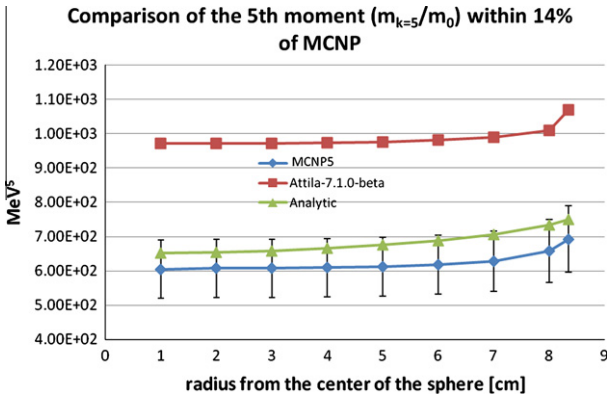

Fig. 11. Comparison plot of the 5th energy moment for the GODIVA benchmark.

Table 6
List of the Rp_n's, Er_n's and w_n's.

Rp_n's	Er_n's	w_n's
1.25E+12	1.00E+06	5.00E+22
6.50E+11	3.00E+06	1.70E+18
1.00E+10	4.00E+06	9.00E+16
2.10E+10	5.00E+06	9.00E+16
1.10E+10	6.00E+06	4.00E+16
1.50E+10	7.00E+06	2.50E+16
9.00E+09	8.00E+06	1.30E+16
8.00E+09	9.00E+06	1.00E+16
5.00E+08	1.00E+07	6.00E+14

$$\left(\frac{a_4}{\widetilde{R}_4}+c_4\widetilde{R}_4+e_4\widetilde{R}_4^3\right)\sin(B_{E4}\cdot\widetilde{R}_4) = -\left(b_4+d_4\widetilde{R}_4^2\right)\cos(B_{E4}\cdot\widetilde{R}_4) \tag{65}$$

$$\left(\frac{a_5}{\widetilde{R}_5}+c_5\widetilde{R}_5+e_5\widetilde{R}_5^3\right)\sin\left(B_{E5}\cdot\widetilde{R}_5\right) = -\left(b_5+d_5\widetilde{R}_5^2+f_5\widetilde{R}_5^4\right)\cos(B_{E5}\cdot\widetilde{R}_5) \tag{66}$$

It turns out the only way for these equations to be equal and have positive amplitudes (the $a_k's$), and positive moments is for the sine and cosine terms to be equal and opposite at $\widetilde{R}_k$. Sine and cosine have equal and opposite values when the B_{Ek} values are $\frac{3\pi}{4\widetilde{R}_k}$, so the set of equations become the following because $sin\left(\frac{3\pi}{4\widetilde{R}_k}\cdot\widetilde{R}_k\right) = -\cos\left(\frac{3\pi}{4\widetilde{R}_k}\cdot\widetilde{R}_k\right)$ and the remaining unknown coefficients, $a_k's$ follow

from working through the algebra of this set of expressions and the amplitudes are positive.

$$a_1 = \widetilde{R}_1 b_1 \tag{67}$$

$$a_2 = \widetilde{R}_2(b_2 - c_2\widetilde{R}_2) \tag{68}$$

$$a_3 = \widetilde{R}_3\left(b_3 - c_3\widetilde{R}_3 + d_3\widetilde{R}_3^2\right) \tag{69}$$

$$a_4 = \widetilde{R}_4\left(b_4 - c_4\widetilde{R}_4 + d_4\widetilde{R}_4^2 - e_4\widetilde{R}_4^3\right) \tag{70}$$

$$a_5 = \widetilde{R}_5\left(b_5 - c_5\widetilde{R}_5 + d_5\widetilde{R}_5^2 - e_5\widetilde{R}_5^3 + f_5\widetilde{R}_5^4\right) \tag{71}$$

The power equation in energy moment form, finding a_0

For any nuclear reactor, the power is a design choice and a known quantity. Power is proportional to the fission rate multiplied by a conversion factor and averaged over the volume of the fueled region of the nuclear reactor. The Power equation below is general and is applicable to any reactor (Lamarsh, pp. 257–258).

C_{fp} is a conversion factor to convert from fissions to Joules.

$$Power = \frac{C_{fp}M_f N_A}{MW_f V}\int_0^\infty \sigma_F(E)\bar{\phi}(E)dE \tag{72}$$

The constants and parameters in Eq. (72) are: *V = volume of the fueled region*, $C_{fp} = 3.2\times10^{-11}\,\frac{joules}{fission}$, *$M_f$ = mass of the fuel*, *MW_f = molecular weight of the fuel*, *N_A = Avogadro's number*, *$\sigma_F(E)$ = energy dependent microscopic fission cross-section* and

$$\bar{\phi}(E) = \frac{1}{V}\int_V \phi(r,E)dV = \textit{volume averaged flux} \tag{73}$$

The volume averaged flux can be isolated and transformed into moment form by multiplying by E^0 inside the volume integral since this is the only part of the expression that has position dependence shown below.

$$\frac{1}{V}\int_V\int_0^\infty E^0\phi(r,E)dEdV = \frac{1}{V}\int_V m_0 dV \tag{74}$$

The moment form of the volume average flux is the 0th moment integrated over the volume

$$\bar{\phi}(E)_k = \frac{1}{V}\int_V m_0 dV \tag{75}$$

The Power equation in moment form becomes Eq. (76)

$$Power = \frac{C_{fp}M_f N_A}{MW_f V}\int_0^\infty \sigma_F(E)\int_V m_0 dVdE \tag{76}$$

The Power equation can be numerically integrated by multiplying the ENDF-VII values with the results of the integrated volume averaged moments ($\bar{\phi}(E)$), where the differential volume for the sphere is $4\pi r^2 dr$.

$$\begin{aligned}\int_V m_0 dV &= 4\pi A_0\int_0^R \frac{\sin\left(\sqrt{C_{E0}}\cdot r\right)}{r}r^2 dr \\ &= 4\pi A_0\left(\frac{\sin(B_{E0}\cdot R)}{B_{E0}^2} - \frac{R\cdot\cos(B_{E0}\cdot R)}{B_{E0}}\right)\end{aligned} \tag{77}$$

If $\widetilde{R}_0 \approx R$ then Eq. (76) becomes Eq. (77)

$$\int_V m_0 dV = \frac{4\pi a_0 R}{B_{E0}} = 4a_0R^2 \tag{78}$$

The power equation becomes Eq. (79).

$$Power_0 = \frac{C_{fp}M_f N_A}{MW_f}\int_0^\infty \sigma_F(E)4a_0R^2 dE \tag{79}$$

Now a_0 is shown in Eq. (80).

$$a_0 = \frac{Power_0 MW_f}{4R^2 C_{fp}M_f N_A\int_0^\infty \sigma_F(E)dE} \tag{80}$$

Each of the constants a_k's, b_k's, c_k's, etc. have a_0 in the numerator so when these constants are normalized a_0 is divided out, for the purposes of this paper power can be set is such a way that a_0 is 1.

Normalized energy dependent neutron diffusion moments

The set of moments that are plotted for comparison are the normalized moments. The moments m_k = 1, 2, 3, 4, 5 are normalized by the 0th moment, m_0. The normalized moments provide information about the population density function i.e. mean energy (m_1/m_0), variance of the energy (m_2/m_0), skewness (m_3/m_0) and kurtosis (m_4/m_0). The normalized energy dependent neutron diffusion moments (NEDNDM) are seen in Eqs. (81)–(86), where a_0 = 1. The set of normalized moments, m_k/m_0:

$$\frac{m_0}{m_0} = \frac{a_0\frac{\sin(B_{E0}\cdot r)}{r}}{a_0\frac{\sin(B_{E0}\cdot r)}{r}} \equiv 1 \tag{81}$$

$$\frac{m_1}{m_0} = \frac{a_1\sin(B_{E1}\cdot r)}{a_0\sin(B_{E0}\cdot r)} + \frac{b_1\cdot r\cdot\cos(B_{E1}\cdot r)}{a_0\sin(B_{E0}\cdot r)} \tag{82}$$

$$\frac{m_2}{m_0} = \frac{a_2\sin(B_{E2}\cdot r)}{a_0\sin(B_{E0}\cdot r)} + \frac{b_2 r\cos(B_{E2}\cdot r)}{a_0\sin(B_{E0}\cdot r)} + \frac{c_2 r^2\sin(B_{E2}\cdot r)}{a_0\sin(B_{E0}\cdot r)} \tag{83}$$

$$\begin{aligned}\frac{m_3}{m_0} = &\frac{a_3\sin(B_{E3}\cdot r)}{a_0\sin(B_{E0}\cdot r)} + \frac{b_3 r\cos(B_{E3}\cdot r)}{a_0\sin(B_{E0}\cdot r)} + \frac{c_3 r^2\sin(B_{E3}\cdot r)}{a_0\sin(B_{E0}\cdot r)} \\ &+ \frac{d_3 r^3\cos(B_{E3}\cdot r)}{a_0\sin(B_{E0}\cdot r)}\end{aligned} \tag{84}$$

$$\begin{aligned}\frac{m_4}{m_0} = &\frac{a_4\sin(B_{E4}\cdot r)}{a_0\sin(B_{E0}\cdot r)} + \frac{b_4 r\cos(B_{E4}\cdot r)}{a_0\sin(B_{E0}\cdot r)} + \frac{c_4 r^2\sin(B_{E4}\cdot r)}{a_0\sin(B_{E0}\cdot r)} \\ &+ \frac{d_4 r^3\cos(B_{E4}\cdot r)}{a_0\sin(B_{E0}\cdot r)} + \frac{e_4 r^4\sin(B_{E4}\cdot r)}{a_0\sin(B_{E0}\cdot r)}\end{aligned} \tag{85}$$

$$\begin{aligned}\frac{m_5}{m_0} = &\frac{a_5\sin(B_{E5}\cdot r)}{a_0\sin(B_{E0}\cdot r)} + \frac{b_5 r\cos(B_{E5}\cdot r)}{a_0\sin(B_{E0}\cdot r)} + \frac{c_5 r^2\sin(B_{E5}\cdot r)}{a_0\sin(B_{E0}\cdot r)} \\ &+ \frac{d_5 r^3\cos(B_{E5}\cdot r)}{a_0\sin(B_{E0}\cdot r)} + \frac{e_5 r^4\sin(B_{E5}\cdot r)}{a_0\sin(B_{E0}\cdot r)} + \frac{f_5 r^5\cos(B_{E5}\cdot r)}{a_0\sin(B_{E0}\cdot r)}\end{aligned} \tag{86}$$

The normalized moments or simply called moments for the rest of the paper are plotted in Figs. 7–11 in the Results and discussion section of the paper. There are three curves in Figs. 7–11: in blue the MCNP moment, in red the Attila moment and in green the analytic moment.

Results and discussion

The plots in Figs. 7–11 below show the comparison of the moments from the three methods (MCNP5, Attila and Analytic). Moments were generated from MCNP5 by creating concentric spheres at roughly 1 cm radii away from each other, so for the MCNP model, nine spheres were modeled so a tally could be made at roughly 1 cm increments up to the edge of the sphere (8.35 cm). The MCNP5 tallies are *f*2 tallies over each surface and each tally was broken into 1000 evenly spaced energy bins up to 10 MeV. Energy bins from 10 MeV to 20 MeV showed large relative errors > 20% and were omitted due to limits in computer power the authors have access to for this work (i.e. a 64-bit laptop with a hex core processor and 6 gigabytes of RAM). To get relative errors below 5% for energy bins from 1E−11 to 10 MeV the number of particles tracked in the MCNP model was 6 million. The *f*2 tally

data in each energy bin was then put in an excel spreadsheet and the various moments were computed numerically based on the definitions already presented for the mean, variance, skewness, kurtosis and higher order moments. Computing times for the MCNP5 calculations were roughly a day, 26.3 h, and Attila computation times were 3–4 h for a normal mesh of 0.01 cm which gave about 100,000 mesh nodes. The reason for the day time frame for MCNP was due to the high number of energy bins and particle histories needed to get in the 5% error range for the 1000 bins in the MCNP case.

Attila moments are created from the 30 group cross-section file radion5 created by Transpire Inc. (energy bins are in Table 1). The data to create energy moments from Attila are from a custom report created in Attila where a line edit was made to collect the flux in each energy group at approximately 1cm increments up to the system edge to match the MCNP5 sphere surface tallies. The points along the line edit from Attila are not exactly 1cm apart but close enough because each point lined up on a mesh point. The flux data in each energy group are numerically calculated similar to the MCNP5 method where the data was put in an excel spreadsheet and integrated according to the definitions already presented for the mean, variance, skewness, kurtosis and higher order moments. The reason why the Attila moments are higher than the MCNP moments are because they are tuned to the fission spectrum which should give an expected mean energy value of about 1.98 MeV (Lamarsh and Baratta, 2001, p. 87) for a sphere of pure ^{235}U. The higher order moments should be higher valued than MCNP because of the fission spectrum weighting. Researchers (Sevast'yanov et al., 2000) claim that the fission spectrum for ^{235}U could be a superposition of five exponential functions and these researchers calculated an average energy value of 1.475 MeV ± 3.77%. As mentioned in the introduction the method of neutron energy moments does not assume a fission spectrum weighting factor which did not shift the values of the moments to that spectrum. Method of neutron energy moments is still diffusion based which is not perfect but the comparison plots show a good agreement with the transport codes general shape, meaning the faster neutrons populate the edges of the system or leak out because of the longer diffusion length or streaming effect of these fast neutrons.

The interesting thing about the analytic moments is that they start to peel away from the MCNP moments right around 3 mean free paths from the boundary of the sphere, about 5 cm (if 1.1cm is taken to be the average mean free path) and then correct back to the boundary value, due to the transport correction factor, r_o. Diffusion theory is valid in finite media at points that are more than a few mean free paths near the edge of the medium (Lamarsh, 1966, p. 129). The limitation of diffusion theory near the boundary of a source is noted and is not valid near the boundary which why it is transport corrected (Glasstone and Sesonke, 1967, p. 112). Even though diffusion theory has its limits the results agree very well with MCNP, the industry gold standard. For multiphysics-engineering type calculations having a continuous energy solution quickly only14% off in the highest moment that is within engineering limits i.e. 20% is an excellent benefit that can be very useful to see multiphysics effects on nuclear reactors.

The shape of the functions for MCNP and Attila are very similar, the Attila moment functions have a sharper up turn and less of a parabolic shape which the analytic and MCNP moments have. The reason for this could be the group structure of the radion5 neutron cross-section file. The authors do not have control over this file and are thankful for the use of the code from Transpire Inc.

The dominate functional shapes that form the constants, CE's for the moments are from the last two summation terms in $F(E)$, see Eq. (16). If the resonance region was not included it would not have changed the value of the analytic moments much for this case, because the contribution from the resonance summation was much smaller than the transition and fast region summations in Eq. (16). This makes sense for a fast reactor such as the theoretical sphere analyzed in this paper. The summation over index l from Eq. (16) does not contribute to the average energy (moment 1) at all and little to moments 2–5. A different functional shape might be more suited to fit the data better in this energy range, but the fit of $F(E)$ to the ENDF-$F(E)$ is good and the moments compare very well, so it might be that the fast reactor analyzed in this paper does not depend on the resonance region, so it would not affect the moment values. More work still needs to be done to see how reliable the method is for a broader set of reactor types.

Overall the analytic moments compare well with the two computational platforms; Monte Carlo and the 30-energy group, S_N order, P_N order, finite element code Attila. The higher moments tend to drift away from the MCNP moments and the error bars shows this, where the error range is 5% for the 1st moment to 14% in the 5th moment and no surprises the normalized 0th moment is 1 for all three cases with 0% error, there is not a figure showing this.

The difficulty in finding continuous energy solutions with the multigroup method is the number of group equations to achieve an accurate solution which can be as high as 1000 (Duderstadt and Hamilton, 1976, p. 292). Continually iterating over the integrals of the neutron flux multiplied by the cross-section until convergence is reached can be computationally expensive and Monte Carlo methods are very time intensive as well, although accurate. The method of neutron energy moments shown here is computationally cheap comparatively, only 6 equations to solve and diffusion equations which are relatively quick to solve computationally (Chapra and Canale, 2002) for many numerical methods.

Conclusions and future work

The EDNDE has been reformulated in terms of a moment equation and solved analytically for a 1-D sphere. The analytic moment solution to the EDNDE agrees quite with (MCNP5 and Attila) in terms of showing that the higher energy or faster neutrons populate the outer radius of the sphere where they leak out of the system. This leakage is seen by the upturn of all of the moments for all three solution methods at the outer radii of the sphere. The analytical moment results fall within the error bars associated with MCNP5 results for all moments (0–5) calculated. The analytical moment results are much more accurate than the 30 energy group Attila simulation because of the reasons stated in the Results and discussion section of this paper.

Acknowledgement

The authors would like to thank Transpire INC for use of the Beta version of Attila-7.1 in this research and the tutoring and explanations on how to use their excellent code.

Appendix A. Table of constants for $F(E)$

Appendix A is the list of constants for each functional piece in the summations that make up $F(E)$, Eq. (16). The energies, $Er_{l,m,n}$'s are listed in eV. The $Rp_{l,m}$'s are listed in eV/cm^2. The Rp_n's are listed in eV^4/cm^2. The $w_{l,m}$'s are listed in eV^2. The w_n's are listed in eV^3. Table 4 is the list of Rp_l's, Er_l's and w$_l$'s. Table 5 is a list of Rp_m's, Er_m's and w_m's. Table 6 is a list of Rp_n's, Er_n's and w_n's.

References

Bin-Wan, C., Ring, T.A., 2006. Verification of SMOM and QMOM population balance modeling in CFD code using analytical solutions for batch particulate processes. China Particuology, 243–249.

Casella, G., Berger, R.L., 2002. Statistical Inference, second ed. Wadsworth Group Duxbury, Pacific Grove, CA, USA.
Chapra, S.C., Canale, R.P., 2002. Numerical Methods for Engineers with Software and Programming Applications, fourth ed. McGraw Hill, New York.
Cho, N.Z., 2008. Fundamentals and recent developments of reactor physics methods. Nuclear Engineering and Technology, 25–78.
Duderstadt, J.J., Hamilton, L.J., 1976. Nuclear Reactor Analysis. John Wiley & Sons, United States.
Edwards, H.C., Penney, D.E., 2001. Differential Equations & Linear Algebra. Prentice Hall, Upper Saddle River.
Foster, A.R., Wright, R.L., 1977. Basic Nuclear Engineering, third ed. Allyn and Bacon, Boston.
Glasstone, S., Sesonke, A., 1967. Nuclear Reactor Engineering. D. Van Nostrand Company, New York.
INL NEA/NSC DOC(95)03, 2009. International Handbook of Evaluated Criticality Safety Benchmarks. INL: NEA/NSC.
Institute, K.A., October 1, 2000. Table of Nuclides. Retrieved July 5, 2011, from Table of Nuclides: <http://atom.kaeri.re.kr/>.
Kenny, J.F., 1947. Mathematics of Statistics, second ed. D. Van Nostrand Company, Inc., New York.
Lab, L.A., July 5, 2000. ENDF/B-VII Incident-Neutron Data. Retrieved July 5, 2011, from ENDF/B-VII Incident-Neutron Data: <http://t2.lanl.gov/data/neutron7.html>.
Lab, L.A., 2008. A General Monte Carlo N-Particle Transport Code-Version 5. Los Alamos: Los Alamos National Lab LA-UR-08-8617.
Lamarsh, J.R., 1966. Introduction to Nuclear Reactor Theory. Addison-Wesley, Reading, Massachusetts, USA.
Lamarsh, J.R., Baratta, A.J., 2001. Introduction to Nuclear Engineering, third ed. Prentice Hall, Upper Saddle River, New Jersey USA.
Lewis, E., Miller, W.J., 1993. Computational Methods of Neutron Transport. American Nuclear Society, La Grange Park, IL USA.
Lockheed Martin/Knolls Atomic Power Laboratory, 2002. Chart of the Nuclides and Isotopes 16th Edition. Lockheed Martin/Knolls Atomic Power Laboratory, New York.
Marchisio, D.L., Pikturna, J.T., Fox, R.O., 2003. Quadrature method of moments for population-balance equations. AIChE, 1267–1276.
Marchision, D., Virgil, R.D., Fox, R.O., 2003. Implementation of the quadrature method of moments in CFD codes for aggregation-breakage problems. Chemcial Engineering Science, 3337–3351.
McGraw, R., 1997. Description of aerosol dynamics by the quadrature method of moments. Aerosol Science and Technology, 255–265.
Morry, S., Williams, M., 1972. Neutron flux perturbations due to absorbing foils. Journal of Applied Physics, 6–18.
Sevast'yanov, V., Koshelev, A., Maslov, G.N., 2000. Representation of the fission spectrum of 235U, 239Pu and 252Cf and the reactor spectrum as a superpostition of five inelastic scattering functions. Atomic Energy, 292–299.
Weinberg, A.M., Wigner, E.P., 1958. The Physical Theory of Neutron Chain Reactors. The University of Chicago Press, Chicago.